

HERA: a high-resolution pan-European hydrological reanalysis (~~1950~~1951-2020)

Aloïs Tilloy¹, Dominik Paprotny², Stefania Grimaldi¹, Goncalo Gomes¹, Alessandra Bianchi¹, Stefan Lange², Hylke Beck³, [Cinzia Mazzetti](#)⁴, Luc Feyen¹

5 ¹European Commission, Joint Research Centre, [\(JRC\)](#), Italy

²Potsdam Institute for Climate Impact Research (PIK), Member of the Leibniz Association, Potsdam, Germany

³King Abdullah University of Science and Technology (KAUST), Thuwal, Saudi Arabia

10 *Correspondence: Aloïs Tilloy (alois.tilloy@ec.europa.eu)*

[⁴European Centre for Medium-Range Weather Forecasts \(ECMWF\), Reading, United Kingdom](#)

Abstract

Since 1950, ~~European rivers have been put under increasing pressure by~~ anthropogenic activities, ~~resulting in changes in~~ have altered climate, land cover, soil properties ~~and~~ channel morphologies. ~~These evolving environmental conditions can translate into~~ and water management in the river basins of Europe. This has resulted in significant changes in hydrological conditions. The availability of consistent estimates of river flow at global and continental level is a necessity to assess and attribute changes in the hydrological cycle. To overcome limitations posed by observations (incomplete records, inhomogeneous spatial coverage), we simulate river discharge for Europe for the period ~~1950~~1951 – 2020 using a state-of-the-art hydrological modelling approach. We use the new European set up of the OS LISFLOOD model, running at 1 arcminute (≈ 1.8 km) with six-hourly time steps. The hydrological model is forced by climate reanalysis data (ERA5-land) that is bias-corrected and downscaled to the model resolution with gridded weather observations. The model also ~~ingests~~incorporates 72 surface ~~fields~~field maps representing catchment morphology, vegetation, soil properties, land use, water demand, lakes and reservoirs. Inputs related to human activities are evolving through time to emulate societal changes ~~in society~~. The resulting Hydrological European ReAnalysis (HERA), provides six-hourly river discharge for 282,521 river pixels with an upstream area > 100 ~~km²~~100 km². We assess its skill using ~~29012,448~~ river gauging stations distributed across Europe. Overall, HERA delivers satisfying results, ~~with~~ (median KGE' = 0.55), despite a general ~~weak~~ underestimation of observed mean ~~dischargedischarges~~ (mean bias = -13.1%), and ~~flow variability. We find thatdemonstrates~~ the capacity to reproduce statistics of observed extreme flows. The performance of HERA increases through time ~~between 1950 and 2020~~with catchment size, as well as varies in space depending on reservoir influence and model calibration. The fine spatial and temporal resolution ~~result~~results in an enhanced performance compared to ~~other~~previous hydrological reanalysis based on OS LISFLOOD for small-to-medium-scale catchments (100- 10,000 km²), ~~with degraded performance remaining for~~

~~small catchments.~~ HERA is the first publicly available long-term, high-resolution hydrological reanalysis for Europe. Despite its limitations, it enables the analysis of hydrological dynamics related to extremes, human influences, and climate change at a continental scale while ~~keeping~~maintaining local relevance. It also creates the opportunity to study these dynamics in ungauged catchments across Europe.

Introduction

In the last century, Europe has experienced a growth in its population, economy and ~~urban~~urbanized area (Li et al., 2021; Paprotny and Mengel, 2023). Recent decades also witnessed a rapid rise in global air temperature, attributable to anthropogenic activities (IPCC, 2023). These evolving conditions have significantly changed flows in European streams and rivers, leading to multiple challenges for hydrological sciences, related, for example, to long term variability, climate change, extremes or human alterations of the water cycle (Blöschl et al., 2019b). ~~To understand~~In order to assess the impacts of these changes, hydrologists need consistent, reliable and long hydrological series. Observations, despite continuous improvements (Blöschl et al., 2019a; Ekolu et al., 2022), are still lacking at a high enough spatial density across Europe and are often uncertain and discontinuous. One option to overcome these limitations is to rely on a suit of models (climate, hydrological, land use) to simulate past hydrological conditions and interpret changing dynamics in the hydrological cycle in connection with rapidly changing human systems (e.g., Richards and Gutierrez-Arellano, 2022). This article introduces the Hydrological European ReAnalysis (HERA) for the period ~~1950~~1951-2020, providing consistent estimates of river flow for European rivers at unprecedented spatial and temporal resolution.

Hydrological models are essential tools ~~when it comes~~ to understand and characterise processes related to the water cycle (e.g., flood and drought forecasting). In the past three decades, there ~~has~~have been efforts in developing models that are able to simulate hydrological processes at large scale (continental to global scale). A myriad of these Global Hydrological Models (GHMs), differing in their conceptualization, now exist (Beck et al., 2017; Sood and Smakhtin, 2015; Kauffeldt et al., 2016; Prudhomme et al., 2011). The nature of GHMs implies that they are usually run at coarse spatial resolution (e.g., 0.5°), limiting their relevance for local and regional water resource problems (Sood and Smakhtin, 2015). Nonetheless, the development of GHMs has been fuelled by continuous improvements in remote sensing technologies and processing power (Yang et al., 2021). Remote sensing technologies now provide high resolution input for hydrological models such as land use and vegetation properties. The advancements in computational capabilities ~~and performances of the models~~ also allowhave allowed to refine ~~both~~ the spatial and temporal scale of hydrological models, ~~providing~~enabling a more accurate representation of surface and subsurface processes and reducing

modelling uncertainties (Wood et al., 2011). In this context, HERA falls within a global effort towards the development of hyper-resolution (1 km and below) land surface and hydrological models at continental (Hoch et al., 2023; O'Neill et al., 2021) and global (Hanasaki et al., 2022) scales.

75 A key ~~limitation preventing hindrance~~ to ~~simulate~~ simulating past river flows has been the availability of meteorological inputs for hydrological models. Among potential inputs, climate reanalysis offers several advantages: temporal coverage (typically spanning several decades), numerous, homogeneous environmental variables, and spatial resolution. Reanalysis data are outputs of climate models calibrated on observed data worldwide (Brönnimann et al., 2018). Here we use ERA5-land, the land component of ERA5- (Muñoz-Sabater et al., 2021). A main advantage of ERA5-Land compared to ERA5 is its horizontal resolution, which is 9 km globally, compared to 31 km in ERA5. This enhanced resolution is obtained by downscaling meteorological variables from ERA5. The temporal resolution is hourly as in ERA5. ~~Reanalysis~~ Nonetheless, reanalysis data are obtained from short-term model forecasts and can be affected by forecast errors; ~~they are not observations~~ (Pfahl and Wernli, 2012). ~~Furthermore,~~ variables Variables produced in ERA5 are averages over grid cells. This averaging combined with the relatively coarse resolution of ERA5/ERA5-land often smooths local extremes (Donat et al., 2014, Tilloy et al., 2022). To tackle this issue, we downscale and bias-correct ERA5-land with a gridded observational dataset, EMO-1 (Thiemig et al., 2022) (Section 2.2).

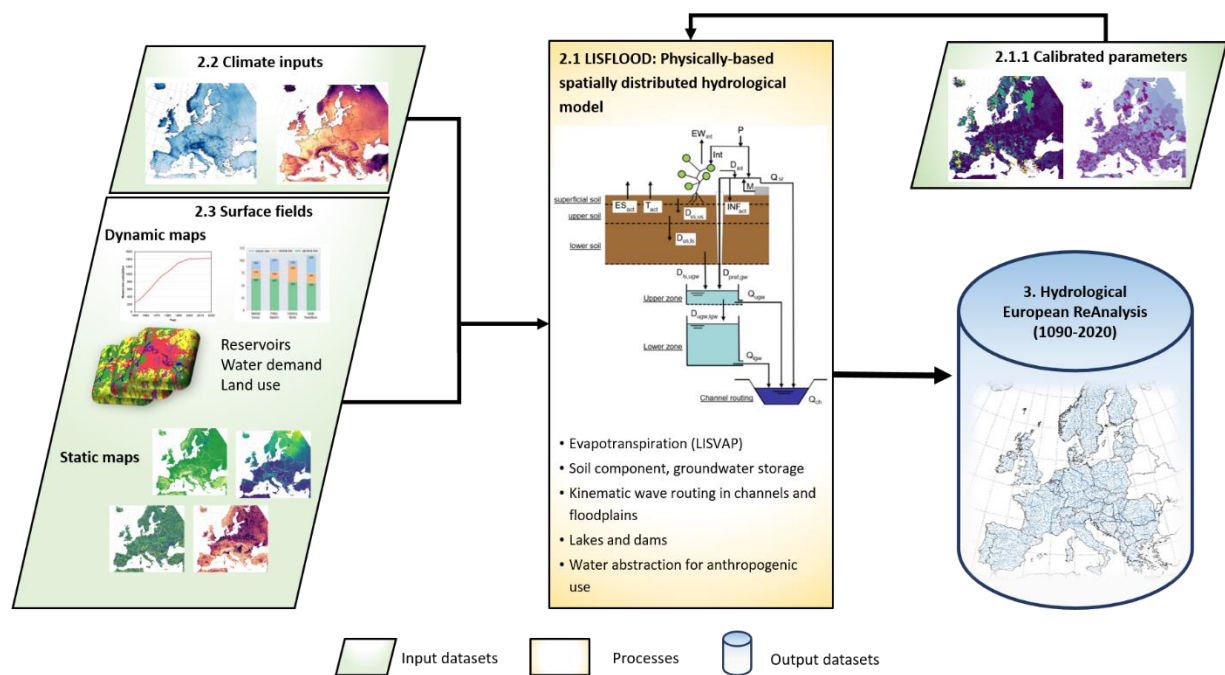
90 In the context of the European Flood Awareness System (EFAS), an operational system for European flood monitoring and forecasting (<https://www.efas.eu>), there ~~has~~ have been recent efforts ~~in recent years~~ to develop more detailed surface fields (e.g., land use, vegetation) (Choulga et al., ~~2023a~~ 2023) and observational climate inputs (Thiemig et al., 2022) at a spatial resolution of 1 arcminute (1', 0.0167°, typically 1.5–3 km² over Europe). These developments come ~~along with~~ alongside improvements on the OS LISFLOOD hydrological model underpinning EFAS. OS LISFLOOD is a spatially distributed grid-based hydrological and channel routing model which was initially developed for flood forecasting and flood risk assessment- (Burek et al., 2013). However, it is also able to model effects of land use change, climate change and river regulation measures ~~(Burek et al., 2013)~~ and has been used in a wide range of hydrological applications, such as mapping population under water stress in relation to how much water is reserved for the environmental environment (Vanham et al., 2021) and projecting droughts in view of climate change (Cammalleri et al., 2020a). It was also used in the generation of the GLOFAS hydrological reanalysis (Harrigan et al., 2020).

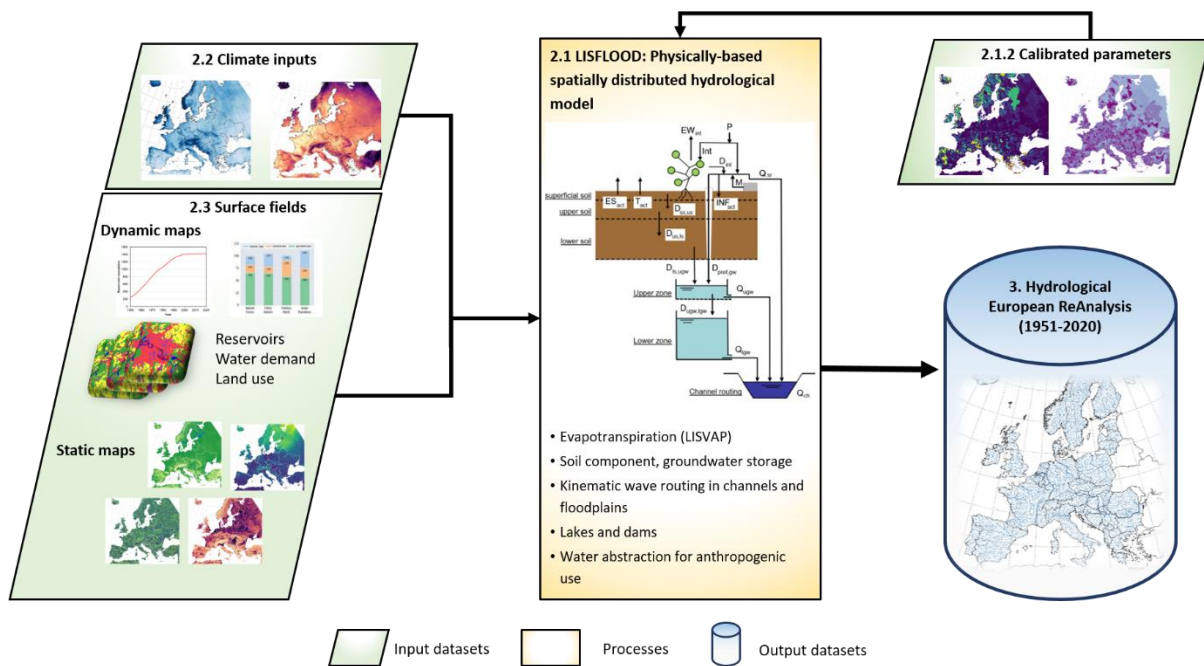
~~This~~ Therefore, tis article brings together improvements from diverse fields (i.e., remote sensing, climate modelling, machine learning, hydrology) to generate a state-of-the-art hydrological reanalysis ~~of Europe~~ for a European domain ~~covering that covers~~ EU27 countries, UK, Switzerland, Iceland, Norway and the Balkan countries (Serbia, Montenegro, Bosnia-Herzegovina, Kosovo, North Macedonia and

Albania) over the past 70 years. HERA aims to reproduce as accurately as possible the evolution of the hydrological landscape of Europe by using the latest development of OS LISFLOOD (Improved improvements in processing speed, spatial and temporal resolutions, calibration), also used in the generation of the latest EFAS v5.0 reanalysis (1991-2022) (Decremer et al., 2023) (Section 2.1). Climate inputs are derived from ERA5-land, bias corrected and downscaled to 1 arcminute to improve the representation of extremes (Section 2.2). We generated dynamic socioeconomic inputs (water demand, land use and reservoir maps) to capture the effect of human activities on the water cycle (Section 2.3). These developments make this simulation dataset the first publicly available long-term Pan-European hydrological reanalysis taking into account the evolving socioeconomic conditions that have altered the continent hydrological cycle since 1950. In Section 3, we assess the performance of HERA against observations from 2901 river gauges in Europe.

Method

The modelling framework developed to generate the HERA dataset is presented in a flowchart in Figure 1. The framework is organized around the OS LISFLOOD hydrological model, which is used to simulate river discharge. For this run, we use calibrated parameters for the European setting of OS LISFLOOD, developed by ECMWF in the context of the EFAS-5 calibration (CEMS-Flood online documentation, 2023). We first introduce the OS LISFLOOD hydrological model and its calibration procedure (Section 2.1). Figure 1 also displays the main input of OS LISFLOOD: high-resolution climate inputs (Section 2.2), state-of-the-art static maps (Section 2.3.1) and dynamic socioeconomic maps (Section 2.3).





130

Figure 1: Flowchart of the framework employed in the generation of HERA. Numbers relate to the section in which each component of the framework is presented.

Hydrological modelling

The OS LISFLOOD model

135

Here, we simulate sub-daily continuous streamflow time series over Europe (**Figure 1**) by means of the OS LISFLOOD model (~~LISFLOOD~~ (Burek et al., 2013; Van der Knijff et al., 2010)). This is a spatially distributed, semi-physical rainfall-runoff model combined with a routing module for river channels (Dottori et al., 2022). The model has been developed by the ~~JRC~~ (Joint Research Centre (JRC) since the late 1990s. ~~The model and~~ is used operationally for large-scale flood forecasting in the European Flood Awareness System (EFAS, efas.eu) and the Global Flood Awareness System (GLOFAS, globalfloods.eu). ~~However,~~ OS LISFLOOD has also been used in drought monitoring (Cammalleri et al., 2020b, 2017), to assess the effect of flood adaptation measures, environmental flow protection, or climate change (Burek et al., 2013; Mentaschi et al., 2020; Vanham et al., 2022). Since 2019, the model is open source and available on [github](https://github.com/ec-jrc/lisflood-code) (GitHub) along with a set of auxiliary tools (<https://github.com/ec-jrc/lisflood-code>). OS LISFLOOD is composed of the following main components:

145

- 3 soil layers (superficial, upper, lower) for water balance modelling;
- sub-models for the simulation of groundwater and subsurface flow (using 2 parallel interconnected reservoirs);
- a sub-model for the routing of surface runoff to the nearest river channel;
- a sub-model for the routing of channel flow.

150

Other processes such as snow melt, infiltration, rainfall interception ~~of rainfall~~, leaf drainage, evaporation and water uptake by vegetation, surface runoff, and exchange of soil moisture between soil

layers are also simulated by the model (OS LISFLOOD ~~OS~~-online documentation, 2023). OS LISFLOOD is also able to model lakes and reservoirs.

155

In this work, we use the latest version of OS LISFLOOD (v4.1.2, January 2023), which includes upgrades compared to previous versions in the hydrological routines and improvements in the modelling of water abstraction for anthropogenic use. Moreover, OS LISFLOOD v4.1.2 benefits ~~off~~from improvements in the management of large inputs and in ~~the~~ computational ~~performances~~performance.

160

Figure 2 displays the domain ~~on~~for which ~~the hydrological simulation is performed, which includes Europe, North Africa and Middle East. However, the data was retained for a smaller domain, comprising~~in HERA. This comprises 42 European countries, ~~excluding and excludes~~ non-EU countries of the former Soviet Union, countries in North Africa and Middle East, and Turkey, ~~resulting that are~~ included in the EFAS domain. Moreover, HERA uses the same domain as the Historical Analysis of

165

Natural Hazards in Europe (HANZE-study) database (Paprotny and Mengel, 2023; Paprotny et al., 2023). We run the model using ~~at~~the 1' grid, ~~which is also~~ used in EFAS-~~5~~ v5.0 (Decremer et al., 2023).

170

The temporal resolution of the simulation is 6-hourly, which is the standard for EFAS since 2020. Due to the size and spatial resolution of our domain combined with the 6-hourly time-steps, we divide the simulations in 71 yearly chunks ~~starting on 3 January 1950 following a 71 year pre-run. Due to~~based

175

on calendar year starting on 3 January 1950. To estimate the initial model state, we performed a 71-years pre-run (longest possible period). More in particular, we used the pre-run to initialize the soil and upper groundwater zone storages and to derive average inflow into the lower zone and discharge, which represent theoretical steady state storage. Due to the rapidly evolving socioeconomic conditions in

180

catchments of Europe, we change the input socioeconomic maps ~~with~~at the start of every new calendar year of the simulation (**Section 2.4**). This differs from the standard EFAS settings, which assume static

185

land use and reservoir network, and only varies the water demand values. At the start of every calendar year, the model is initialized with the state variables from the last time step of the previous year (warm start). River initialization in OS LISFLOOD can lead to unrealistic discharge in some catchments. We

190

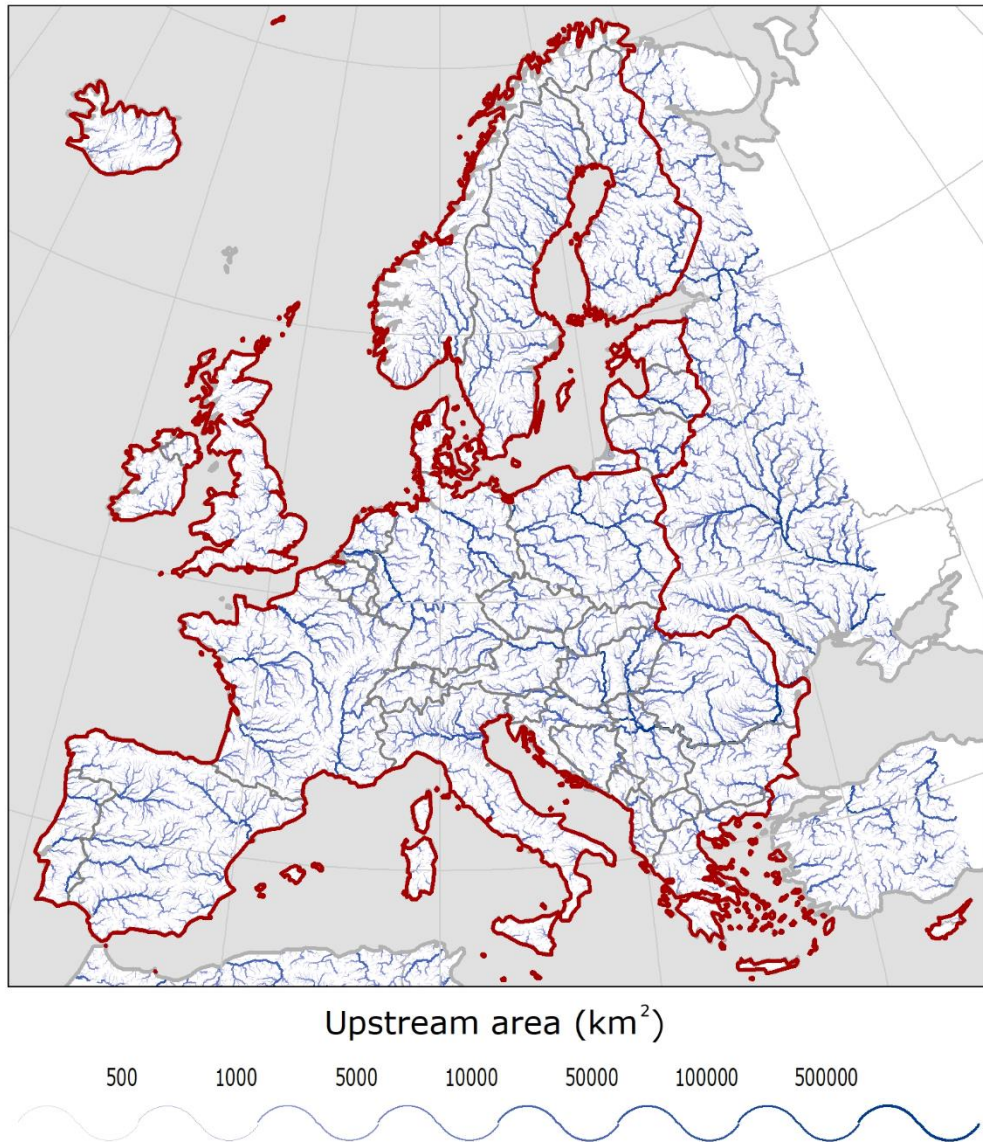
~~retain~~therefore removed the first simulation year (1950) from the final dataset. Further, we only retained simulations for river pixels with an upstream area greater than 100 km², resulting in simulations in the 282,521 river pixels displayed in **Figure 2**.



Upstream area (km²)

500 1000 5000 10000 50000 100000 500000





185

Figure 2 River network (rivers with an upstream area > ~~100~~100 km²) on which discharge data has been generated. The HERA domain (in which data is provided) is confined by the red bordered area.

Model Calibration

190

In this work, we also take advantage of the new EFAS-~~5~~v5.0 calibration that was completed in December 2022 by ECMWF. The calibration was performed using the EMO-1 meteorological dataset (Thiemig et al., 2022) over the period 1990-2021. ~~Daily and/or six hourly data discharge at a total of,~~ with a focus on high flows. The modified Kling-Gupta Efficiency (KGE', Gupta et al., 2009; Kling et al., 2012) was used as a skill metric. Discharge data at 1903 stations, identified through a selection process based on several criteria (CEMS-Flood online documentation, 2023)), were used to calibrate the LISFLOOD model over Europe. Sub-daily data is always preferred when available (994 over 1903 stations). For stations where only daily observations were available, the 6 hourly discharge simulations

195 were first aggregated to daily steps (daily mean) before evaluating the objective function. The calibration was performed at catchment level, with ~~catchments of~~ the 1903 selected stations ~~entailing covering~~ 69.6% of the HERA domain, ~~a. A~~ map showing the ~~extent of~~ calibrated and ~~uncalibrated~~ catchments is provided in **Supplementary Figure S1**. The calibration ~~has been~~ was performed on 14 parameters that influence the modelling of snow melt, water infiltration into the soil, surface water flow, groundwater flow, lakes and reservoirs dynamics. ~~These parameter were allowed to vary within physically realistic ranges.~~ A list of the calibration parameters is provided in **Supplementary Table S1**. Parameter values were identified using the Distributed Evolutionary Algorithm for Python (DEAP, Fortin et al. 2012) within a physically realistic range. The calibration protocol went from head-catchments to downstream catchments in a top-down manner, prescribing physical dependencies between upstream and downstream catchments within the same basin.

Coastal and endorheic catchments with drainage area smaller than 150 km², representing 6.5% of the HERA domain, are modelled with default parameter values. Parameter values for other ungauged catchments were estimated by parameter regionalisation. These catchments are mostly located near the coastlines, with a high concentration in southern Italy and Greece, and represent 23.9% of the HERA domain. The parameter regionalization here consists ~~in~~ of transferring parameter values (except the ones linked to reservoirs and lakes) from a calibrated catchment to an ungauged catchment. Catchments are matched according to climatic and geographical similarities (Beck et al., 2016). We discuss the impact of calibration on the skill of HERA in Section 3.1.1. For more information on the calibration of ~~EFA-SEFAS v5.0~~, we refer to the online documentation of the Copernicus Emergency Management Service for floods (CEMS-Flood online documentation, 2023).

Climate inputs: Bias-adjusted climate reanalysis data

To force the hydrological model OS LISFLOOD, we ~~used~~ a ~~modified version of~~ bias-adjusted and downscaled climate dataset based on the ERA5-land climate reanalysis ~~dataset ERA5-land~~ (Muñoz-Sabater et al., 2021). The main steps involved in the preparation of the climate inputs are summarized in **Figure 3**. The following variables are retrieved from ERA5-land at hourly temporal resolution for 1950-2020:

- Total precipitation (tp)
- Mean temperature (ta)
- Mean zonal and meridional wind speed (u, v)
- Mean dew point temperature (td)
- Total surface solar radiation downwards (ssrd)

Precipitation and temperature data were aggregated to 6-hourly resolution, and the other variables to daily resolution (**Figure 3**). All variables were averaged, except precipitation, which was summed to reach the target temporal resolution. Minimum and maximum daily temperature were also calculated, while dew point temperature was converted into relative humidity and actual vapour pressure.

~~ERA5 Land data is too coarse for the grid resolution used in LISFLOOD (section 2.1), which~~
Our setting of OS LISFLOOD requires meteorological data with a 1' resolution. To downscale ERA5-Land data from $0.1^\circ = 6'$ to 1', we ~~therefore~~ performed a statistical downscaling and bias adjustment using ISIMIP3BASD v3.0.0 (Lange 2019, Lange ~~2022~~et al. 2024, Frieler et al. 2024). The ISIMIP3BASD method was initially developed for phase 3 of the Inter-Sectoral Impact Model Intercomparison Project (ISIMIP) and aims to provide robust bias adjustment of extreme values, preservation of trends across quantiles, and a clearer separation of bias adjustment and statistical downscaling compared to its predecessors (Lange, 2019). ~~Particularly the robust bias adjustment of extremes is relevant in the context of this analysis. We use~~We used the new EMO-1 gridded observational dataset (1' version of EMO-5, Thiemig et al. 2022) developed for the operational EFAS-~~5v5.0~~ as the high-resolution reference dataset. EMO-1 covers the period 1990–2020 and has also been used directly as climate inputs ~~for~~in the calibration ~~of LISFLOOD (Section 2.1.2).~~ We ~~use~~used 1990–2020, ~~where both datasets overlap,~~ as the training period for the algorithm. ~~since both datasets overlap for this period.~~ The trained algorithm is then applied to ERA5-Land to produce high-resolution data for both the training period and for 1950–1989, where high-resolution data comparable to EMO-1 are not available. The resulting climate data consistently ~~cover~~covers 1950–2020. The ISIMIP3BASD method is applied on the following variables:

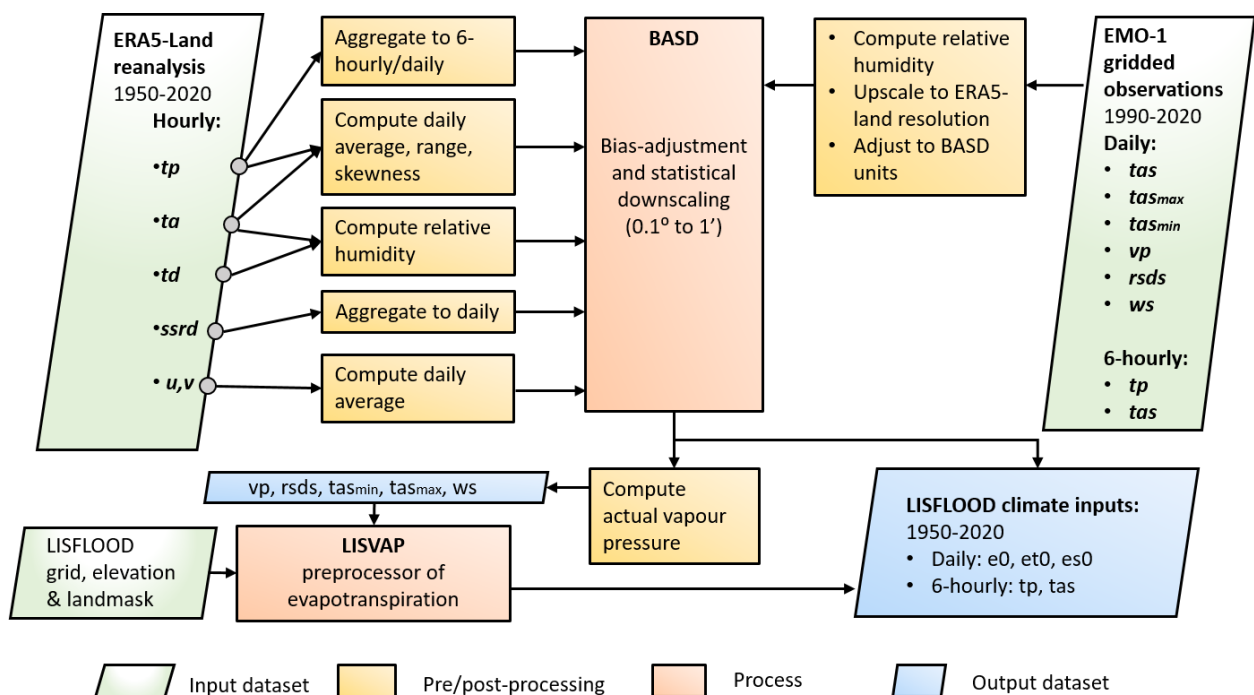
- daily mean near-surface relative humidity (hurs), obtained from actual vapor pressure (vp),
- daily and 6-hourly total precipitation (pr),
- daily total surface downwelling shortwave radiation (rsds),
- daily mean near-surface wind speed (ws),
- daily and 6-hourly mean near-surface air temperature (tas),
- diurnal near-surface air temperature range ($tasrange = tasmax - tasmin$),
- diurnal near-surface air temperature skewness ($tasskew = (tas - tasmin)/tasrange$).

Here, $tasmin$ and $tasmax$ are the daily near-surface air temperature minimum and maximum, respectively.

Version 3.0.0 of ISIMIP3BASD differs technically from version 2.5.0 that was used to produce the climate forcing data for phase 3b of the Inter-Sectoral Impact Model Intercomparison Project (ISIMIP3b, Frieler et al. 2024), yet both versions produce the same results, and we apply version 3.0.0 using the same climate variable-specific parameter settings as for the ISIMIP3b data production (Lange

265 ~~2024~~et al. 2024, Frieler et al. 2024). ISIMIP3BASD ~~was initially has been~~ designed ~~to be applied to~~for
 daily data. ~~In order but it is applied here~~ to bias-adjust and statistically downscale sub-daily (6-hourly
 pr and tas) data, ~~we apply ISIMIP3BASD independently to every 6 hour period of~~ ~~as if these are daily~~
~~values. For the day and merge the results in post-processing.~~ The bias adjustment ~~part of ISIMIP3BASD~~
 270 ~~is~~, a parametric trend-preserving quantile mapping method. ~~Parametric quantile mapping is~~ ~~was~~ applied
 to pr, sfcwind, tas, and tasrange. ~~Non,~~ while non-parametric quantile mapping ~~is~~ ~~was~~ applied to hurs,
 rsds, and tasskew. The bias adjustment ~~is~~ ~~was~~ done at the spatial resolution of ERA5-Land, 6', using
 spatially aggregated EMO-1 data- (spatial averaging). Data resulting from the bias-adjustment ~~are~~ ~~were~~
 then statistically downscaled to 1' spatial resolution by using ~~the statistical relationships between EMO-~~
~~1 data at 1' and 6'~~an algorithm based on the MBCn bias-adjustment method (Cannon et al., 2018)
 275 (Figure 3). The downscaling method is conservative in the sense that the 1' output data would be
 identical to the 6' input data ~~if we in case the former is~~ spatially aggregated ~~the former~~ back-up to 6'
 resolution.

Finally, potential evapotranspiration (e_0), potential open-water evapotranspiration (e_0) and potential
 280 bare soil evapotranspiration (e_{s0}) are computed with bias-adjusted and downscaled data at pixel level
 using an approach based on the Penman-Monteith equation with the LISVAP model (LISVAP online
 documentation, 2023).



285 **Figure 3: Climate inputs pre-processing scheme, including temporal aggregation, bias-adjustment, statistical downscaling and processing of evapotranspiration.**

Surface field maps

~~To accurately represent hydrological processes,~~ LISFLOOD requires a set of surface fields maps. Depending on the model set-up, ~~LISFLOOD~~ it can ingest up to 108 surface fields divided in six categories:

- 290 (i) Catchment morphology and river networks
- (ii) Vegetation cover types and properties
- (iii) Soil properties
- (iv) Land use
- (v) Water demand
- 295 (vi) Lake and reservoir information

The first three categories, ~~thereafter~~ hereafter referred to as static maps, ~~are~~ were directly taken from the CEMS_SurfaceFields_2022 open-source dataset of the Copernicus Emergency Management Service, developed for the European domain at 1 arc min resolution, which can be found in the JRC Data Catalogue (Choulga et al., ~~2023b~~–2023). The last three ~~last~~ categories ~~are~~ were derived from 300 CEMS_SurfaceFields_2022 and modified to take into account socioeconomic changes (hereafter referred to as dynamic socioeconomic maps). This section briefly presents each of the ~~previously enumerated~~ map categories, with an emphasis on dynamic socioeconomic maps, which are original to this work.

Static maps

305 Static maps include surface fields of morphology and channel shapes (14 maps), vegetation properties (18 maps) and soil properties (29 maps).

Morphology and river network information ~~are~~ were directly used for the computation of snow melting, temperature scaling, river routing and open water evapotranspiration. Morphologic information ~~is~~ was 310 derived from elevation and includes elevation gradient, within-grid standard deviation of elevation ~~within-grid,~~ and Manning's roughness coefficient. Maps representing channel shapes and river networks provide information on grid cell area (which ~~vary~~ varies with latitude as the grid projection is WGS84), local drainage direction, upstream area and channel dimensions. All morphology and river network maps ~~are~~ were derived from the Multi-Error-Removed Improved-Terrain Digital Elevation 315 Model v.1.0.3 (MERIT DEM) (Yamazaki et al., 2019) and the Catchment-based Macro-scale Floodplain (CaMa-Flood) Global River Hydrodynamics Model v4.0 maps (Yamazaki, 2023).

Vegetation cover types and property maps are involved in the computation of precipitation interception, evaporation, transpiration, surface runoff and root water uptake. These properties are described though 320 four variables: crop coefficients (transpiration), crop groups (water uptake), manning roughness

(surface runoff) and leaf area index (interception and evaporation). Each of these ~~variable are variables~~ were mapped for three different land cover types: forest, irrigated and other. ~~Maps~~ Further, maps of planting and harvesting days for rice, which has specific water demands, are also available. Vegetation properties ~~are were~~ derived from several data sources including the Copernicus Global Land Service (CGLS) Leaf Area Index (LAI) ~~at 1 km~~ (Copernicus, 2021), the Spatial Production Allocation Model (SPAM) – Global Spatially-Disaggregated Crop Production Statistics Data for 2010 (Yu et al., 2020; International Food Policy Research Institute, 2019), and the Food and Agriculture Organisation (FAO) of the United Nations Irrigation and Drainage Paper No.56 (Allen et al., 1998).

Soil properties refer to physical characteristics of the soil and aim to describe the water dynamics through a vertical soil profile. In OS LISFLOOD, the soil profile is composed of three layers: superficial (0 – 5cm), upper (5 – varying (30 – 50) cm) and lower soil layer. For each layer, ~~variable variables~~ representing soil hydraulic properties (e.g., soil moisture content, pore size index) are provided. Similarly to vegetation ~~properties property~~ maps, variables ~~are were~~ mapped for ~~different two categories~~ of land cover ~~type, here forest, 'forest' and other 'other'~~. Soil properties ~~are computed were derived~~ from ~~a global dataset~~, the International Soil Reference and Information Centre (ISRIC) ~~SoilGrids250m~~ global gridded ~~soil 386 information~~ SoilGrids dataset (release 2017) available at 250m (Hengl et al., 2014), which is based on more than 150,000 observation sites and covariate data.

A table summarizing all the static and dynamic surface ~~fields field~~ maps used ~~in this piece of work to produce HERA~~ is provided in **Supplement Table S2**. For more details on ~~the these~~ surface fields maps, their production and input datasets used, we refer to (Choulga et al., ~~2023a~~ 2023).

Dynamic land use

OS LISFLOOD includes six ~~classes of~~ land use classes as inputs: rice, other irrigated land, forest, sealed surfaces, open water, and other (non-irrigated agriculture, non-forest natural, pervious artificial), ~~which~~; these land use classes are mostly based on CLC-Refined 2006 dataset by Batista e Silva et al. (2013) in the default setting. ~~Intereception~~ Among hydrological processes, interception, evapotranspiration, infiltration, and surface runoff respond differently to each land use type. With the aim to better represent complex rainfall-runoff processes, OS LISFLOOD accounts for the sub-grid variability in land use. Therefore, the spatial distribution of each land use class is defined as a percentage of the whole represented area of a given pixel (~~LISFLOOD OS online documentation, 2023~~). ~~We modify~~ OS LISFLOOD online documentation, 2023). The magnitude of the variation of hydrological response is tied to the magnitude of the changes in land cover. De Roo et al., (2001), for instance, investigated the effects of land use changes on floods in two European catchments and identified different results depending on the magnitude of the land cover change. While such changes tend to have a limited impact on river discharge, they can locally increase flood magnitude (Merz et al., 2021;

[Sajikumar and Remya, 2015; Van Lanen et al., 2013; Van Loon, 2015](#)). We modified here the grid cell fractions of each land use class using HANZE-Exposure land use maps at 100 m resolution (Paprotny and Mengel, 2023) for 42 countries in the study area. In the remaining part of the domain, we ~~used~~ coarser, 5' resolution maps from HYDE 3.2 (Klein Goldewijk et al., 2017) to modify the 2006 values. The temporal evolution of land area of each class is displayed in **Figure 5.a**. There has been a strong increase in sealed surfaces (+40%), while for the other relevant land use classes the changes are less than 10%, with ~~increases in~~ more land occupied by irrigated agriculture (except rice), water surface (due to reservoir construction) and forests.

365 **Dynamic water abstraction**

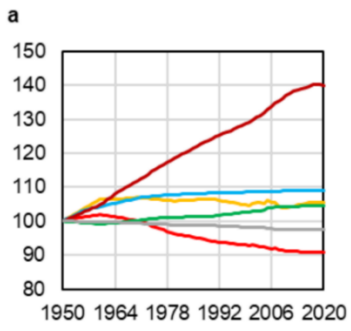
Human water use, representing water withdrawal from the natural environment (e.g., rivers, reservoirs, groundwater) for human needs, is grouped ~~into~~ four main sectors: livestock, domestic, manufacturing industry, and energy production. ~~Within~~ LISFLOOD, water use is supplied by surface water bodies and groundwater depending on the sector (Choulga et al., ~~2023a~~, 2023). A considerable increase in water abstraction in a region can diminish surface water resources within the same area. The model also accounts for groundwater abstraction for human use, except for flooded irrigation and cooling processes. Increased groundwater abstraction can locally reduce (or halt) baseflow. To derive monthly historic sectoral water withdrawal maps, we followed the methodology of Huang et al., (2018) and used ~~by~~ the Food and Agriculture Organization (FAO) AQUASTAT sectoral water withdrawal data (~~FAO~~ [Food and Agriculture Organisation](#), 2023) as a starting point. These data were subsequently spatially and temporally disaggregated using a variety of datasets. These include the Global Human Settlement Layer (Schiavina et al., 2019; Florczyk et al., 2019) for population estimates, the Global Change Analysis Model (GCAM; Calvin et al., 2019) for regional water withdrawal and electricity consumption, and the Gridded Livestock of the World (GLW; Gilbert et al., 2018) for livestock distribution. Additional datasets included the Multi-Source Weather (MSWX; Beck et al., 2022) for air temperature data, United States Geological Survey (USGS) water withdrawal estimates, and Vassolo and Döll (2005) industrial and thermoelectric withdrawal maps. More information on water demand and input datasets used is provided in Choulga et al. (~~2023a~~ 2023).

385 We extrapolated the water withdrawal maps to the period 1950-1978 using annual gridded 0.5 degree data from ISIMIP 3a (Frieler et al., 2024; Wada et al., 2016) that were downscaled to 1' resolution using historical population data from HANZE (Paprotny and Mengel, 2023) and HYDE 3.2 (Klein Goldewijk et al., 2017) for other parts of the domain. More precisely, the ratio between EFAS high-resolution water demand maps and the ISIMIP 3a dataset for 1979 was used to adjust water withdrawal data in each grid cell. Intra-annual (monthly) cycling of water use in the energy and domestic sectors was estimated for 1950–1978 using the same approach as for 1979–2020, informed by temperature data

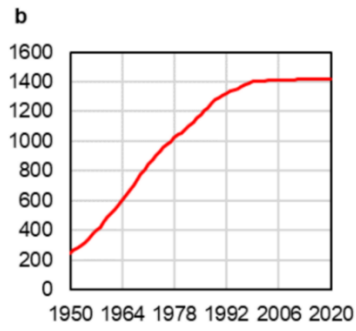
from our input meteorological dataset (**section 2.3.1**). Livestock water use ~~iswas~~ assumed constant before 1979. Water demand and use for irrigation ~~iswas~~ computed directly by the hydrological model based on land use data and available water. The evolution of water use by sectors between 1950 and 2020 is displayed in **Figure5.c** ~~as well as Supplementary Table S4. Total water use peaked in 1990 after more than doubling since the 1950s, before declining due to a drop in demand from manufacturing and energy sectors. Nonetheless, there are usually much stronger trends at country or catchment levels.~~

Dynamic reservoir maps

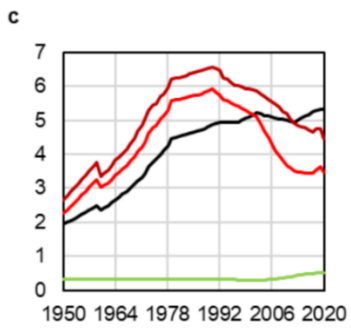
~~Maps on reservoirs~~ Reservoir maps contain the location and an identifier of reservoirs and are linked to tables containing information metadata on storage capacity, construction year and a set of values associated to reservoir operation rules ~~of operations in LISFLOOD~~. Normal reservoir outflow rates were ~~also~~ further adjusted through the model calibration (**Section 2.1.2**). The year of construction for each reservoir was taken from the EFAS reservoirs database, HANZE (Paprotny and Mengel, 2023), Global Reservoir and Dam Database (GRanD) v1.3 (Lehner et al., 2011), or additional manual research for reservoirs not covered by the three datasets. The reservoir maps are updated every simulation year (January 1st) by adding newly built reservoirs. **Figure4** ~~When a reservoir is added, it is considered as empty and fills up according to its associated metadata. Figure5.b~~ shows the evolution of the number of reservoirs in Europe during the period 1950 – 2020. The number of reservoirs in the model increased six-fold from 244 in 1950 to 1419 in 2020, though few were built since the late 1980s. ~~Total water use peaked in 1990 after more than doubling since the 1950s, before declining due to a drop in demand from manufacturing and energy sectors. Nonetheless, there are usually much stronger trends at country or catchment levels.~~



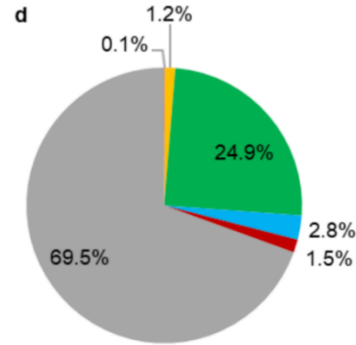
— Rice — Irrigated
 — Forest — Water
 — Sealed — Other



— Reservoirs



— Domestic — Energy
 — Industry — Livestock



■ Rice ■ Irrigated ■ Forest
 ■ Water ■ Sealed ■ Other

415

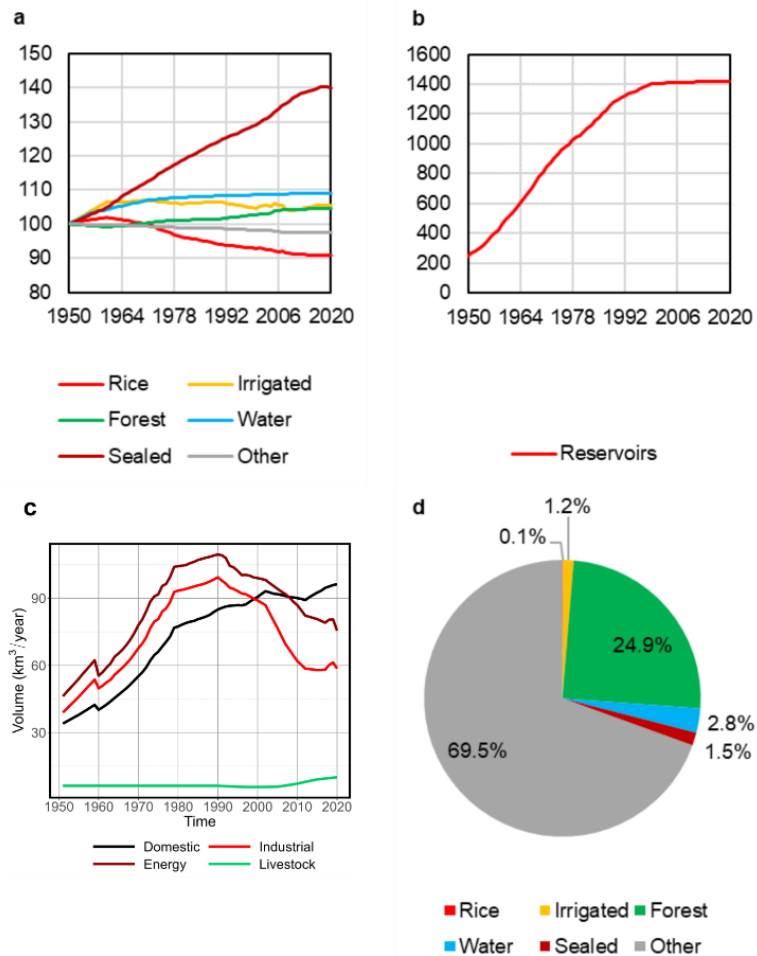


Figure 4: Variation in socioeconomic inputs in the hydrological model, ~~average for~~ averaged over the entire EFAS domain: (a) land area by use category, 1950=100, (b) number of existing reservoirs, (c) water demand by sector in mm per grid cell per year, (d) shares of land use between the different classes in 2020.

420 Results

Technical validation

425 ~~To evaluate~~ We evaluated our hydrological reanalysis, ~~we use by comparison against a dataset of~~ daily river discharge observations from ~~34423,442~~ stations across Europe. ~~The~~ Of the data ~~were~~ were obtained ~~for~~, 60% were from the Global Runoff Data Centre (GRDC) and ~~for~~ 40% from national public datasets of France, Norway, Poland, Spain, Sweden and the United Kingdom. Furthermore, this dataset was compiled independently from the one used in the EFAS calibration (**Section 2.1.2**). The stations' record duration ~~vary~~ varies between 1 ~~year~~ and 71 years. The selection of stations used for validation is based on several criteria:

- 430 • Spatial matching: ~~to~~ To link stations to ~~its~~ their corresponding river pixel, we ~~scan~~ scanned the nine modelled pixels around the river gauge location. When information on the upstream area was available (for 60% of the river gauges, retaining stations), we retained the pixel with the closest upstream area to the reported one. For pixels without information on the upstream area,

435 ~~we retained~~ the one with the closest simulated mean discharge (Q_{mean}) to the observed one. ~~A total of 398 stations did not match with river pixels, mostly due to their upstream area being lower than 100km². For For~~ a more accurate spatial matching, we ~~use, when used the~~ available LISFLOOD coordinates from the EFAS calibration (1026 stations). ~~A total of 546 stations did not match with LISFLOOD river pixels, mostly due to their upstream area being lower than 100 km².~~

- 440
- ~~Upstream area verification: The spatial matching selected the closest upstream area for stations where we have information on catchment area. It is however possible that the reported catchment differs largely from its matched pixel upstream area. We removed stations where the difference between the pixel and observed upstream area was larger than 50% (51 stations).~~
 - Mean discharge comparison: For some stations, the ratio between observed and simulated Q_{mean} ~~were was~~ suspicious. This could be due to an erroneous spatial match (i.e., matching of a river with a station on a tributary). As uncertainty grows with smaller streams, we ~~decided~~ decided to remove ~~those~~ with a suspicious Q_{mean} ratio ($r_{Q_{\text{mean}}} > 6$ or $r_{Q_{\text{mean}}} > 3$ if $Q_{\text{mean,obs}} > 10 \text{ m}^3/\text{s}$) (~~10349~~ stations)
 - ~~Based on model skill (KGE, See below), we identify~~ Manual check: A manual verification was performed on 66 stations with low skill, and remove the ones where the distance between the ~~KGE~~ $KGE < -0.41$. Each station and its corresponding matching pixel exceeds 2.5 km (25 stations). With this process, we may remove valid spatial matches, however, we put an emphasis on eliminating faulty matches, as these could bias the conclusion ~~were~~ individually checked, resulting in the removal of the validation.
 - Finally, a manual check was performed on 74 stations with $KGE < 0.41$, removing 2413 more stations due to wrong spatial ~~match~~ matching, erroneous station location, and doubtful observations. ~~The corresponding river pixel was manually set for 8 stations. Manually checked stations and the reason for their exclusion/inclusion are provided in Supplementary Table S5.~~
 - Finally, we removed stations with a record length shorter than 30 years (334 stations). This enabled a meaningful comparison between different locations in the validation process.

460 This procedure resulted in the selection of ~~29012,448~~ 2,448 river stations across Europe, with an upstream area ranging from 100 to 785,421 km². Among these stations, more than half (~~17581,507~~ 17,507) have an upstream area of less than ~~1000km²~~ 1000 km² and a fifth (~~579) has~~ 498) have an upstream area of less than ~~200km²~~ 200 km².

465 ~~Performance~~ The HERA reanalysis comes at a sub-daily resolution (6-hourly), but the performance could only be evaluated at the daily time step of the observational dataset. Discharge data from HERA was therefore aggregated (daily mean) for the technical validation. We expect performance to be slightly

higher at daily scale is, as the temporal aggregation tends to increase the correlation between observed and modelled discharge. Performance was assessed using the modified Kling-Gupta efficiency metric (KGE', on discharge data (Gupta et al., 2009; Kling et al., 2012). KGE' is used as the standard performance metric in EFAS and GLOFAS (Harrigan et al., 2020; Cammalleri et al., 2020b), but also as well as in other hydrological model assessments (Lin et al., 2019; Harrigan et al., 2020; Beck et al., 2017) and it is composed of three components: correlation, bias errors, and variability errors:

$$KGE' = 1 - \sqrt{(r - 1)^2 + (\beta - 1)^2 + (\gamma - 1)^2} \quad (1)$$

$$\beta = \frac{\mu_s}{\mu_o} \quad (2)$$

$$\gamma = \frac{\sigma_s/\mu_s}{\sigma_o/\mu_o} \quad (3)$$

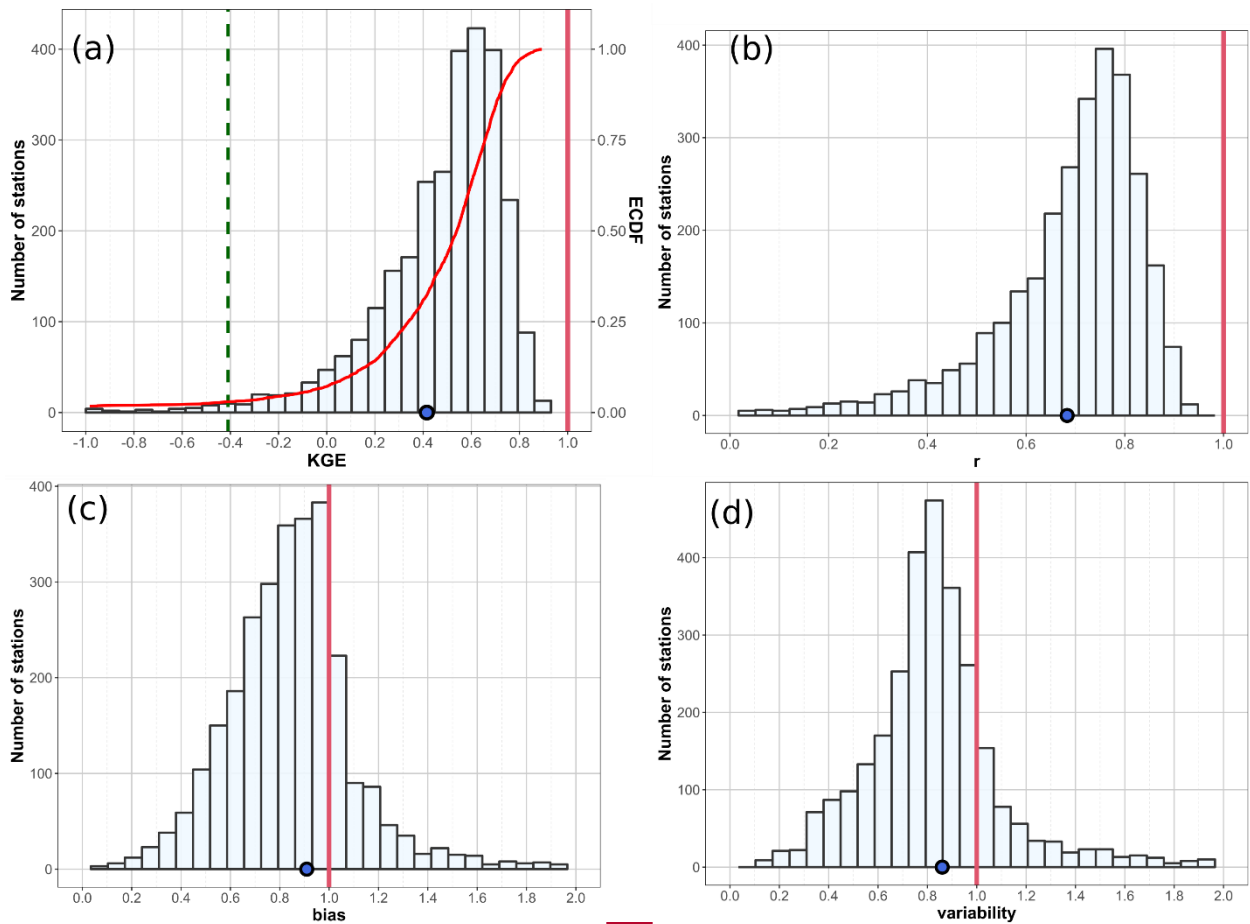
where r is the Pearson correlation coefficient between simulated (s) and observed (o) flow, β is the bias ratio, γ is the variability ratio, μ the mean discharge, and σ the discharge standard deviation. KGE' and its three components are dimensionless with an optimal value on 1. It is important to note here that KGE' values should not be interpreted like the more traditional Nash-Sutcliffe efficiency (NSE, Nash and Sutcliffe, 1970). Indeed, for KGE' the mean flow benchmark has a value of $KGE' = 1 - \sqrt{2} = -0.41$. Any value above -0.41 therefore exceeds the benchmark (Knoben et al., 2019). In Section 3.1.1, we assess model performance across space, time (1950-2020) and catchment size, in order to identify strengths and weaknesses of HERA, meaning that the model performs better than simply taking the mean.

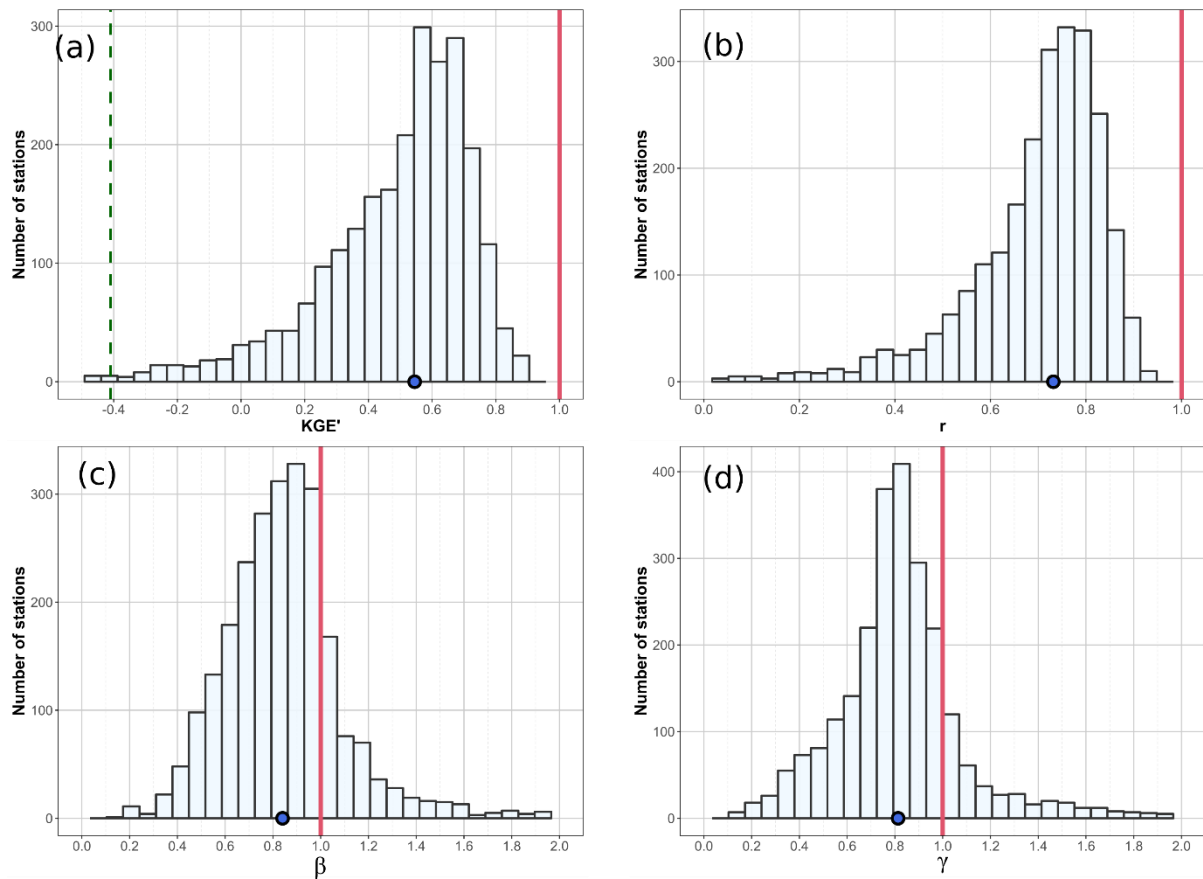
In Section 3.1.1, we assessed model performance across space, time (1951-2020) and catchment size, in order to identify strengths and weaknesses of HERA. Despite covering many aspects of the performance of hydrological models, KGE' mainly focuses on mean values, and give a higher weight to high extremes compared to low ones. As this dataset also aims to be used for long term analysis of hydrological extremes (high and low flows), we also look at evaluated how well extreme-high and low quantile extremes are reproduced, and we compare these performances with the one of median flows. We also assess how well the including their timing and seasonality on annual maxima and minima are reproduced in HERA.

Hydrological performance

We quantify here the overall performance of HERA in terms of KGE' as well as the decomposition of this indicator into its three components: correlation, bias and variability. Figure 5 displays the distribution of KGE' and its three components across the 2,448 validation stations retained. Among these stations, 2,811 (97%) have. We obtained a $KGE' > -0.41$ for 2,411 (98.5%) of them, meaning the reanalysis is skilful for these stations (Figure 5.a). The median KGE' across all

500 catchments is 0.5455 while the mean is 0.4246, although this value varies widely across catchments (Figure 5.a, Figure 6.a). The mean correlation value is relatively high ($\bar{r} = 0.69$) with 8990% of the stations having $r > 0.5$ (Figure 5.b). From Figure 5.c and Figure 5.d, we can observe that there is a tendency to slightly underestimate flows (mean bias ratio = $-8.3\bar{\beta} = -13.1\%$) and flow variability (mean variability ratio = $\bar{\gamma} = -14.72\%$). The bias ranges between 0.8 – 1.2 (0.5 – 1.5) in 51% (8950% (91%) of the river gauges, which is considered as very good for hydrological reanalysis (Harrigan et al., 2020; Alfieri et al., 2020; Lin et al., 2019; Yang et al., 2021).





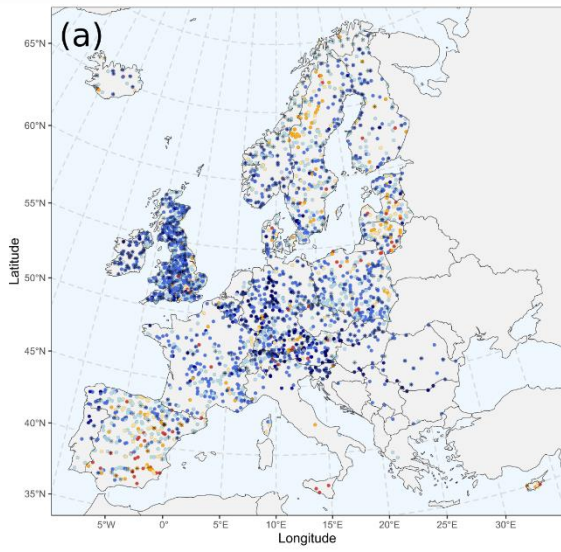
510 **Figure 5:** HERHERA hydrological skill for the 29012,448 selected stations in terms of (a) KGE' and its three components: (b) pearson (r) Pearson correlation, (c) bias ratio, (d) variability ratio. In (a), the green dashed vertical line represent the benchmark KGE' value (-0.41). The red vertical line represents the ideal value values and the blue dot represent represents the mean median for all stations.

515 **Figure 6** shows the spatial performance of the model in terms on KGE' and its components. The highest skill can be observed in central and north-western Europe. The vast majority of stations in UK, Germany, France, Austria, Switzerland (which together account for 4651% of all 29012,448 stations) exhibit a good (>0.5) to very good (>0.75) KGE'. On the other hand, performance is relatively poor in Spain, Cyprus, Southern Italy, Scandinavia and the Baltic countries-Northern Poland. Factors that can explain the poor performances in southern Europe include the combination of arid climates and the strong influence of lakes and reservoirs (Figure 7.c) and their deviation from the temperate climate of central Europe, where best performances are found. In northern Europe and mountainous areas, a lower performance can be attributed to the influence of snowmelt on river flow. Worst performing). Dry catchments are mainly driven by where precipitation events are separated by long dry spells are in

520 general very difficult to model (Cantoni et al., 2022). In Scandinavia, the negative 1.2esbias (Figure 6.c) in Spain and Scandinavia could be linked to an underestimation of precipitation and snowmelt in Scandinavian mountains (Beck et al., 2017, 2020). **Figure 6.d highlights presents** the variability ratio of simulated over to observed flow. Overall, our reanalysis exhibits lower variability than observations, with 8283% of the catchments having a variability ration lower than 1. ratio below one. The

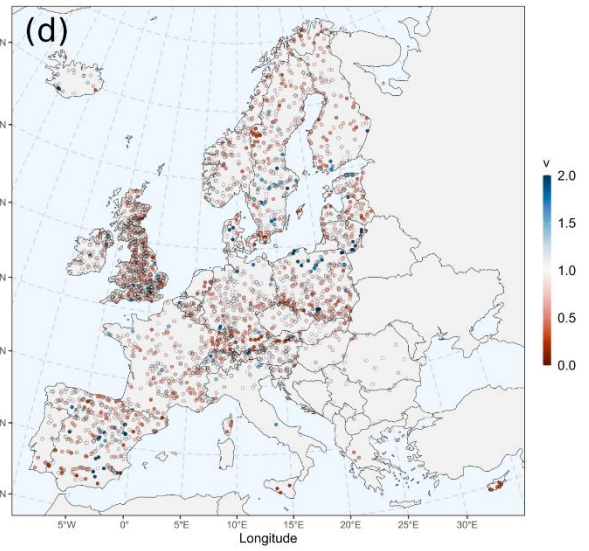
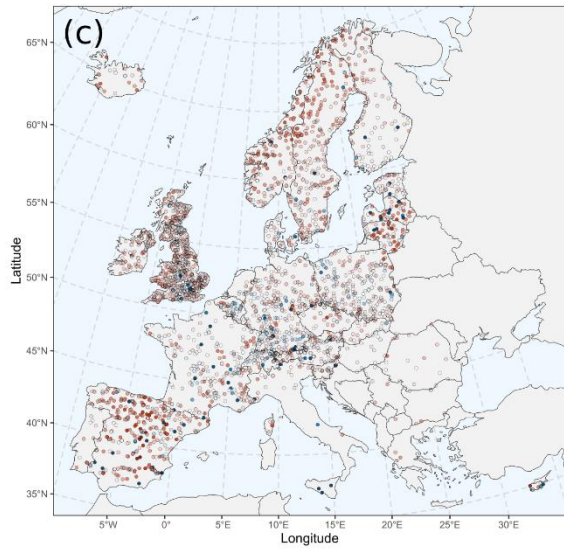
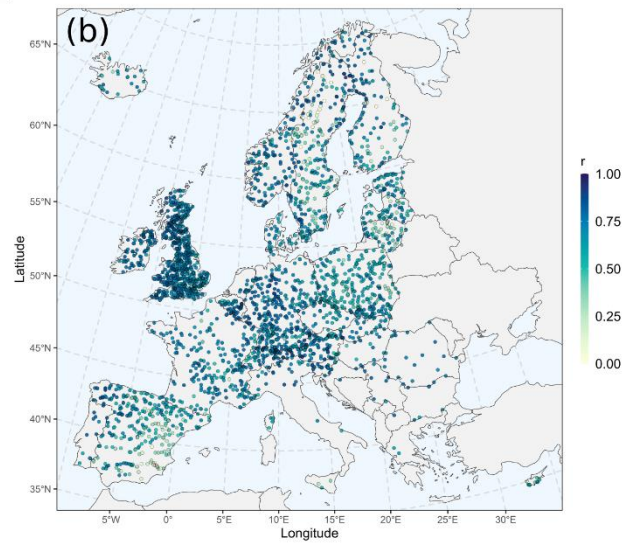
525

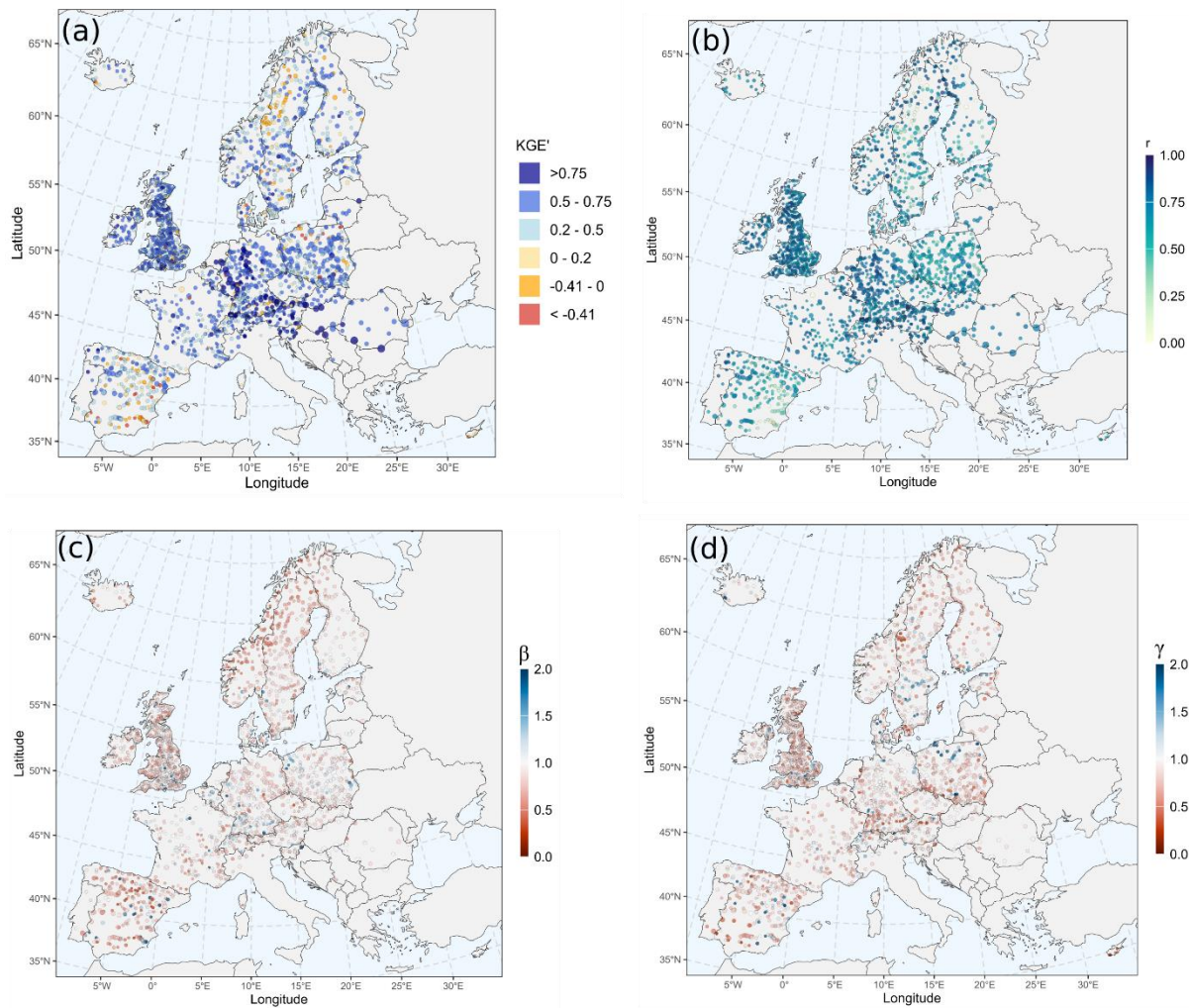
530 underestimation of variability was also found in the EFAS v5.0 run, although it is more pronounced in HERA. This could be explained by the different meteorological forcing used in the two runs.



KGE

● < -0.41	● 0 - 0.2	● 0.5 - 0.75
● -0.41 - 0	● 0.2 - 0.5	● > 0.75





535 **Figure 6: Maps of spatial skill of HER for the 2001 selected stations in terms of (a) KGE' and its three components: (b) Pearson correlation, (c), bias ratio, (d) variability ratio.**

KGE' values and its three components are in line with previous LISFLOOD applications at global (Alfieri *et al.*, 2020; Hirpa *et al.*, 2018) and European level (Zajac *et al.*, 2013; CEMS-Flood online documentation, 2023). However, the 2448 river gauges considered in the improved resolution of the present reanalysis allows comparison with observations in smaller catchments compared validation of HERA. Point size are proportional to global studies catchment size.

540 We validate HERA on stations with a wide range of catchment area (mean upstream area = 7615 of 7.615 km²), where model which has an impact on OS LISFLOOD performance is typically lower (Harrigan *et al.*, 2020-2020). The set of 2,448 validation stations includes stations that were used in the calibration process (596) as well as stations in uncalibrated catchments (36) (See **Supplementary Figure 7-breaks S1**). In **Figure 7**, we break down the performance of the reanalysis according to ~~decades~~ different attributes of each catchment: time (**Figure 7.a**), catchment area (**Figure 7.b**) and), reservoir impact (**Figure 7.c**) and calibration status (**Figure 7.d**).

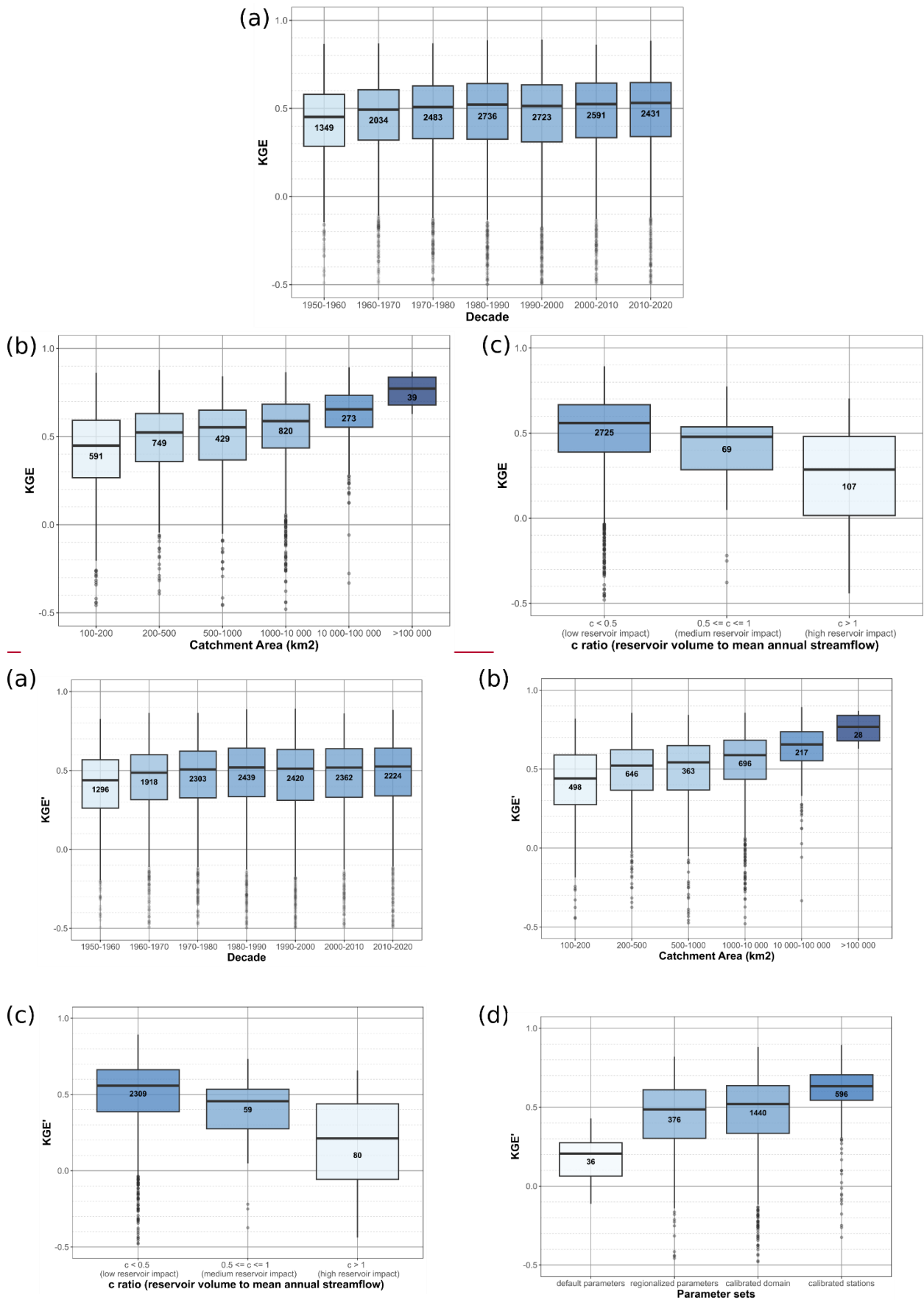


Figure 7: Boxplot of **HERHERA** KGE' according to different classifications of the **2901,2448** river stations used in the validation, (a) time, (b) catchment area and (c) reservoir impacts. Numbers inside boxplot represent the amount of

river gauges for each category, while the colour of the boxplot represent the median performance of the group from low (light blue) to high (dark blue).

555 Overall, the skill of HERA shows a slight increase through time, ~~from a median KGE' value with an~~
~~increase of 0.44 (IQR 0.25–0.57) during 21% of the KGE' med between~~ the 1950s ~~to 0.52 (IQR 0.30–~~
~~0.64)~~ in the 2010s. ~~Skill~~~~The skill~~ increases between ~~1950~~~~1951~~ and 1980 and then stabilizes from
~~1980~~~~1981~~ to 2020, though the results are influenced by changes in gauge data availability over time. It
~~also~~ could ~~also~~ be driven by improved climate inputs. **Figure 7.b** ~~unravel unsurprising yet interesting~~
560 ~~patterns. Model~~~~shows that model~~ skill increases with catchment size, from a ~~median KGE' KGE' med~~ of
0.44 (IQR 0.25 – 0.59) for ~~very small~~~~the 498 smallest~~ catchments ($<200 \text{ km}^2$) to 0.77 (IQR 0.68 – 0.84)
for the ~~3928 largest~~ catchments ~~with an upstream area greater than~~ ($>100,000 \text{ km}^2$ – 000 km^2). Such
patterns have already been observed at global scales (Harrigan et al., 2020). It is important to note ~~here~~
that ~~the~~ majority of stations used in this validation (~~61–62%~~) have an upstream area below
565 ~~1000~~~~km²~~; ~~1000 km² and~~ the median upstream area of the ~~2901~~~~2448~~ stations is ~~597~~~~583~~ km^2 , ~~which. This~~
is half of the median upstream area of the 1903 stations used in the calibration of EFAS-5 (CEMS-
Flood online documentation, 2023).

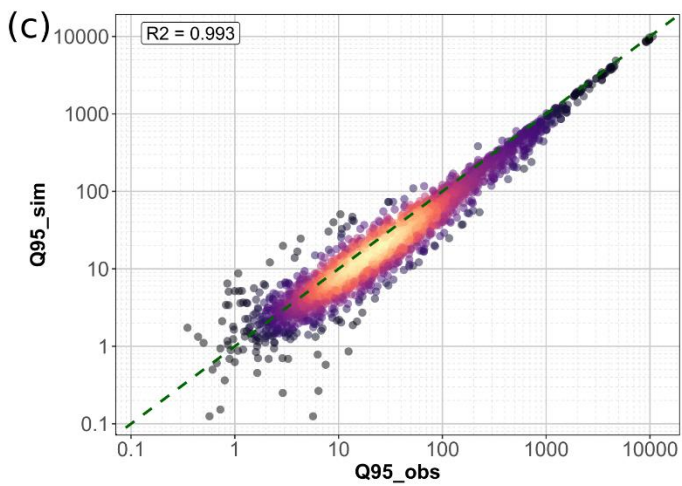
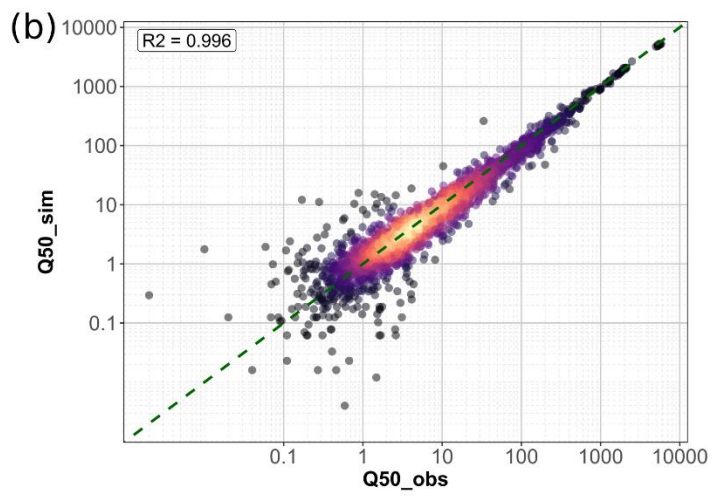
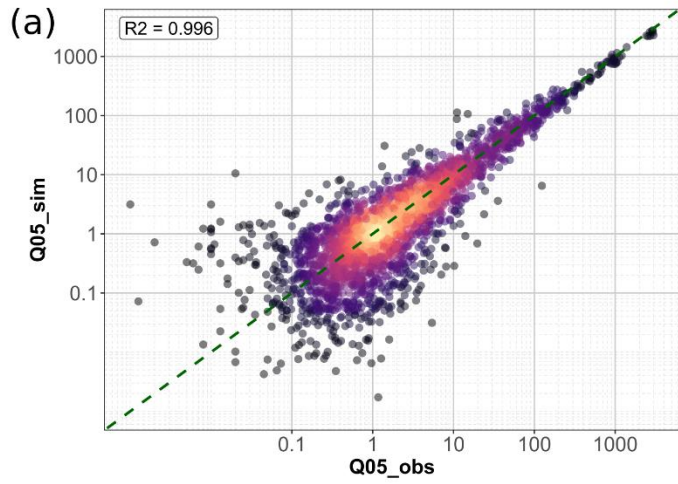
~~Finally, we divide~~~~We also divided~~ stations according to reservoir ~~impacts~~~~influence~~. From the 1420
570 reservoirs active in 2020 (which represent the maximum amount over the considered time window), we
~~estimate~~~~estimated~~ the impact of reservoirs on streamflow at ~~pixel~~~~grid-cell~~ level. This ~~is~~~~was~~ done by
computing the ratio (c [-]) of reservoir volume to mean discharge ~~proposed by~~ (Nilsson et al., 2005) at
every ~~pixel~~~~grid cell~~. The ratio has been computed with the accuflux function from PCRaster and
compares the upstream cumulative reservoir capacity [m^3] and the cell-specific annual volume of annual
575 streamflow [m^3] (Zajac et al., 2017). This ratio varies between 0 and 1608 downstream of
~~embalse~~~~Embalse de~~ Finisterre in central Spain. Most of the river ~~pixels~~~~grid-cells~~ highly impacted by
reservoirs are found in southern Europe, ~~more in particular~~~~particularly~~ in Spain and Bulgaria. **Figure**
7.c highlights the influence of reservoirs on the skill of the reanalysis. River cells affected (medium and
high, $c > 0.5$) only represent 6% of stations and ~~river~~~~pixels~~~~grid cells~~ in the domain (**Figure 12**). Median
580 skill is the lowest for highly impacted ($c > 1$) stations, with ~~a median KGE' of~~~~KGE' med~~ = 0.24 ~~where~~
~~low, whereas minimally~~ impacted stations have a ~~median KGE' KGE' med~~ of 0.55. This highlights the
difficulty of large-scale hydrological models such as OS LISFLOOD to accurately simulate reservoir
outflows (Zajac et al., 2017).

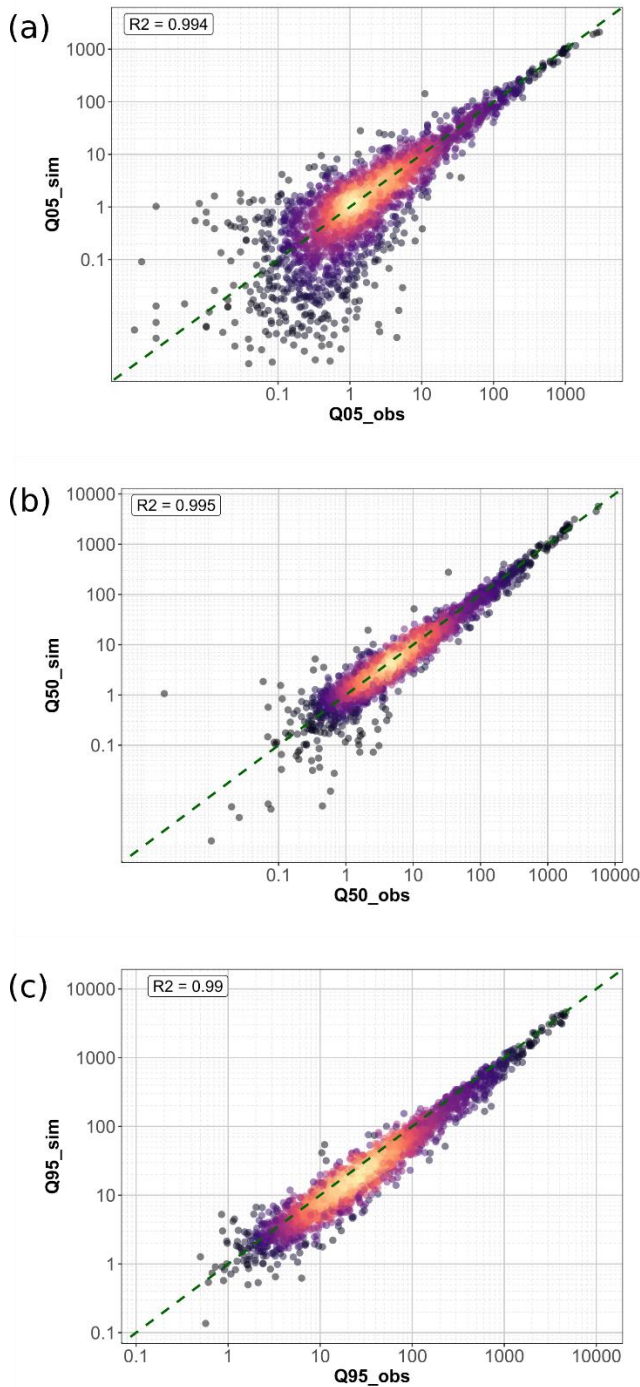
585 ~~Finally, we investigated the influence of calibration on the model skill. In Figure 7.d, River gauges are~~
~~divided into four groups according to their calibration status. As displayed in Supplementary Figure~~
~~S1, 83% of the stations considered in the validation fall into the domain calibrated for EFAS v5.0. We~~
~~find a better performance for calibrated stations, (KGE' med = 0.64) and a comparable skill for stations~~
~~within the calibrated domain (KGE' med = 0.52) and stations benefitting from the parameter~~

590 regionalization ($KGE'_{med} = 0.47$). The performance is much lower for catchments with default parameters, which here are limited to small ($< 150 \text{ km}^2$) coastal and endorheic catchments.

Reproduction of extremes

595 ~~HERA can be used to assess changes in several aspects of European river flows, including average discharges, flow regimes, seasonality (Section 3.1.2). The efforts made in refining both spatial and temporal scale (high resolution, bias corrected) also aim to make HERA suitable for the analysis of extremes. It is notorious that large~~Large scale hydrological models forced by climate reanalysis often fail to reproduce extreme hydrological event characteristics, ~~for example flood magnitudes tend to be typically underestimated in part due to the coarse spatial and temporal resolution~~ (Brunner et al., ~~2021b~~2021; McClean et al., 2023). ~~We~~Here, we analyse ~~here~~ how well HERA reproduces different ~~daily~~ flow quantiles (q05, median, q95) through the Person correlation coefficient (~~r~~) and the coefficient of determination (R^2) (**Figure 8**) ~~for the 2448 considered catchments~~. The ability ~~of the reanalysis~~ to capture annual maxima/minima and their seasonality is also assessed (**Figure 9**).





605

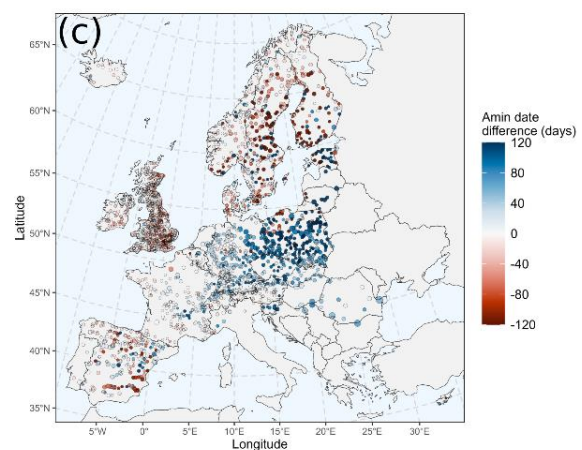
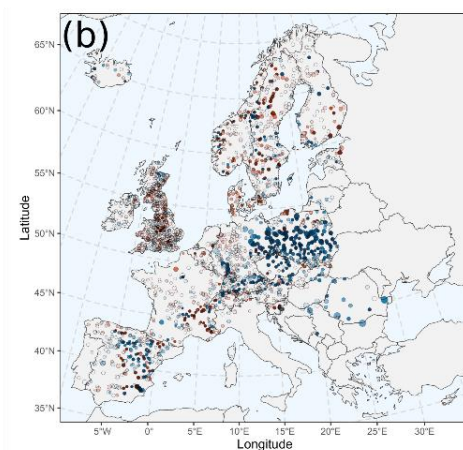
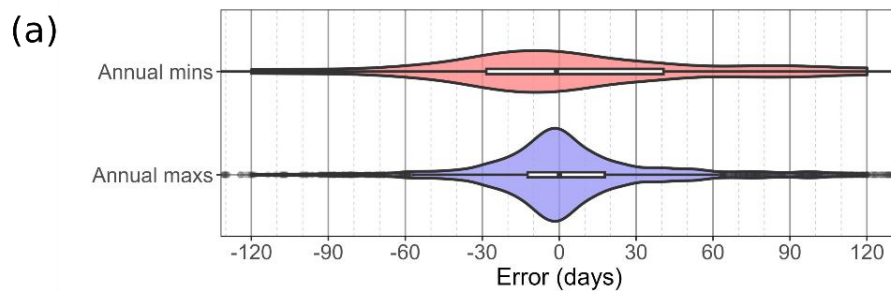
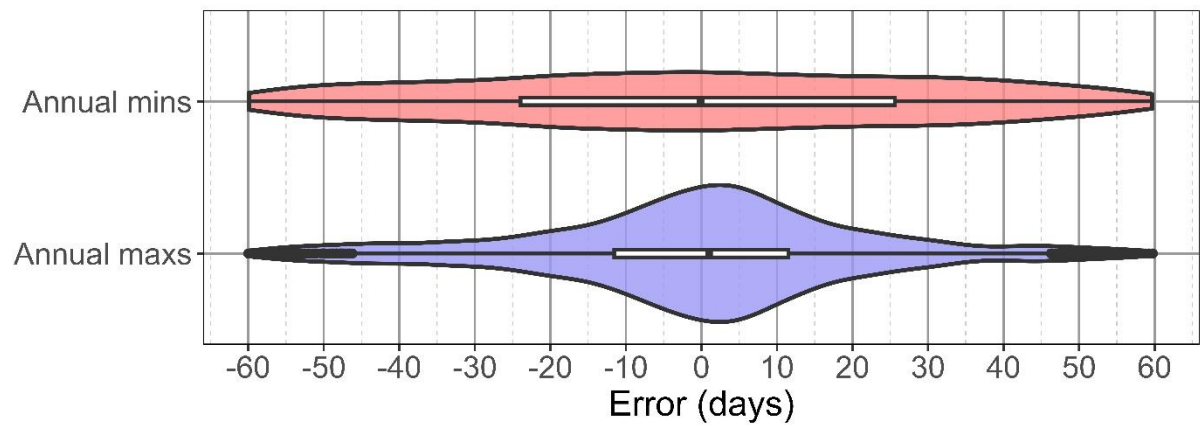
Figure 8: Scatterplot of observed versus simulated daily river flow quantiles [m^3/s^{-1}]: (a) 5% quantile, (b) median (q50), (c) 95% quantile (q95) for the [29012448](#) River gauges.

610

Figure 8 displays scatter plots of observed versus simulated quantiles. Each point represents one of the [29012448](#) stations. From **Figure 8**, we observe that low (5% quantile: Q_{05}) and median (Q_{50}) flows are generally well represented with $R^2 \geq 0.996$ in both cases (Figure 8.a and Figure 8.b), especially for larger discharge values. However, despite this generally good agreement, there is a more pronounced deviation of simulated values from observations for lower flow values, expressed by a higher dispersion for Q_{05} . These deviations can be attributed to errors or biases in our climate

inputs (McClean et al., 2023), ~~in~~ the hydrological model (Feyen and Dankers, 2009), but also to errors
615 in flow measurements, especially for Q_{05} (Despax, 2016; Tomkins, 2014) and anthropogenic impacts
on low and median flow regimes (Brunner, 2021) that are not accurately represented in the model (see
Figure 78.c). The number of stations with large deviations in the reproduction of high flow statistics
(Q_{95}) is minor compared to Q_{05} and Q_{50} . Nonetheless, despite a relatively high R^2 (0.99399), there is a
620 general underestimation ~~bias~~ in the simulated values (**Figure 89.c**). ~~As mentioned above, such~~
~~underestimation biases are~~, which is common for large scale hydrological models. Similarly to low and
median flows, errors in ~~low~~high flow statistics can be due to ~~biases~~bias and smoothing of extremes in
~~our~~ climate inputs and errors in ~~the~~ hydrological modelling. Furthermore, it has been shown that using
KGE' for calibration purposes can result in an underestimation of peak flows (Brunner et al.,
~~2021b~~2021). Uncertainty associated to flow measurements also play a major role for high flows, as
625 rivers discharge are usually not directly measured during floods (Despax, 2016). Finally, ~~both~~the spatial
and temporal ~~resolutions~~resolution of ~~our~~the model can affect its ability to reproduce high flows,
particularly for flash floods in small catchments.

We also assessed the ability of the reanalysis ~~into~~ reproduce the timing of annual maxima and minima
630 ~~events~~of discharge as well as their overall seasonality. ~~Figure 9~~As the daily temporal scale is not the
~~most relevant when it comes to drought analysis with discharge data (Hannaford and Marsh, 2006;~~
~~Kohn et al., 2019), annual minima were computed from 30-day moving average flows. Figure 10.a~~
displays the ~~errors~~mismatch in mean day of occurrence computed with circular statistics following ~~the~~
~~method explained in~~ (Berghuijs et al., (2019). We observe that the median error in the mean day is
635 very close to zero for both maxima (median = 0.1, IQR = -11 - 12 - 18) and minima (median = -1, IQR
= -25 - 2528 - 41), but with ~~more~~a much higher dispersion for ~~drought~~annual minima compared to
~~floods. This can be linked to different drivers and characteristics~~the annual maxima. The higher
dispersion for low flows is due to the slow-onset nature of these events (Brunner et al., 2021), ~~with~~
~~droughts being slow onset events lasting longer than flood events (Van Loon, 2015). Despite some~~
640 ~~outliers (mostly located in north-eastern~~2021a). **Figure 10.b** shows the difference in timing between
~~simulated~~ and ~~south-eastern Europe, not displayed here), seasonal errors~~observed annual maxima across
the 2448 considered stations. Differences in timing are ~~reasonable for both floods~~smaller over the
Atlantic coast though a particularly high lag (simulated maxima delayed by 30 days or more in HERA)
is observed over Poland and ~~drought events~~central Spain. For low flows (**Figure 10.c**), delays in
645 ~~central Europe are larger than 30 days, while in Scandinavia the timing can be up to several months too~~
~~early. This can be explained by the high hybridity of river regimes (several high and low flow seasons)~~
~~in these regions, which may be captured with varying accuracy in HERA.~~



650

Figure 9: Assessment of the ability of HERA to reproduce the timing of annual maximum and minimum flows. (a) Violin plot of error in mean day of occurrence of annual maxima/minima (daily discharge) and minima (30-day averaged discharge) computed with circular statistics. Inside each violin plots, boxplots display the median, 1st and 3rd quantiles. (b) Difference between the modelled and observed mean annual maxima date (positive value means a later occurrence in HERA). (c) Difference between the modelled and observed mean annual minima date (positive value means a later occurrence in HERA)

655

In addition to the validation protocol presented in this section, we carried out a comparison between HERA and another recent hydrological simulation done with the grid-based conceptual mesoscale Hydrological Model (mHM) (Kumar et al., 2013; Samaniego et al., 2010; Thober et al., 2019) for Europe for the period 1960-2010. More details on the comparison are provided in Supplementary material (Figure S3-S6).

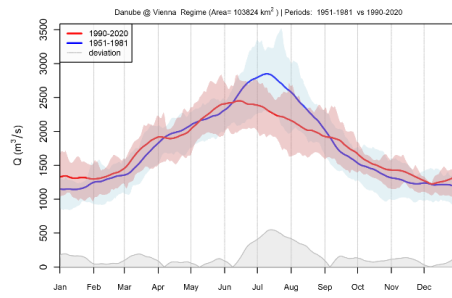
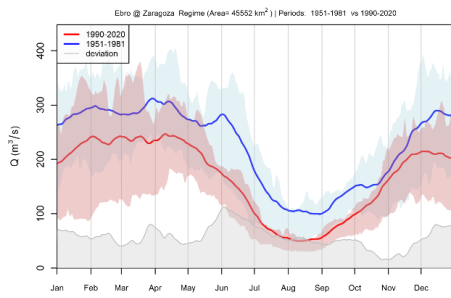
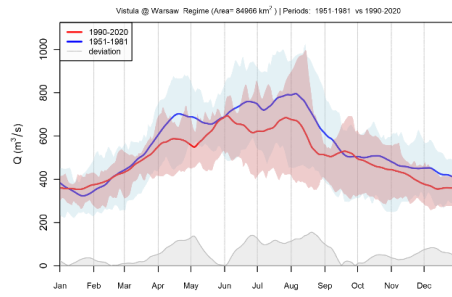
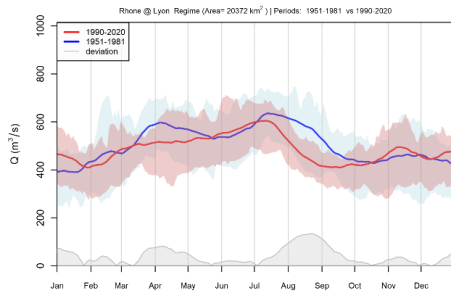
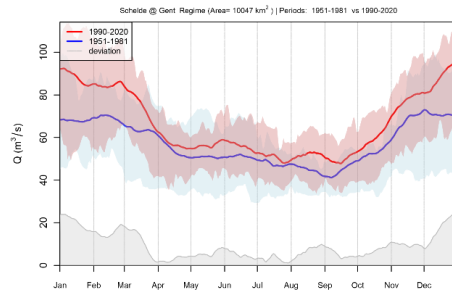
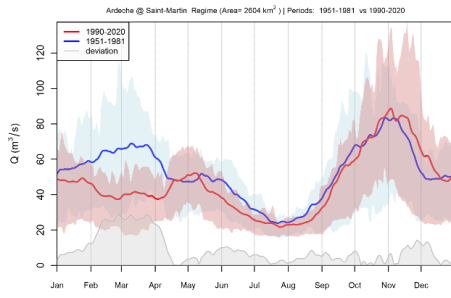
660

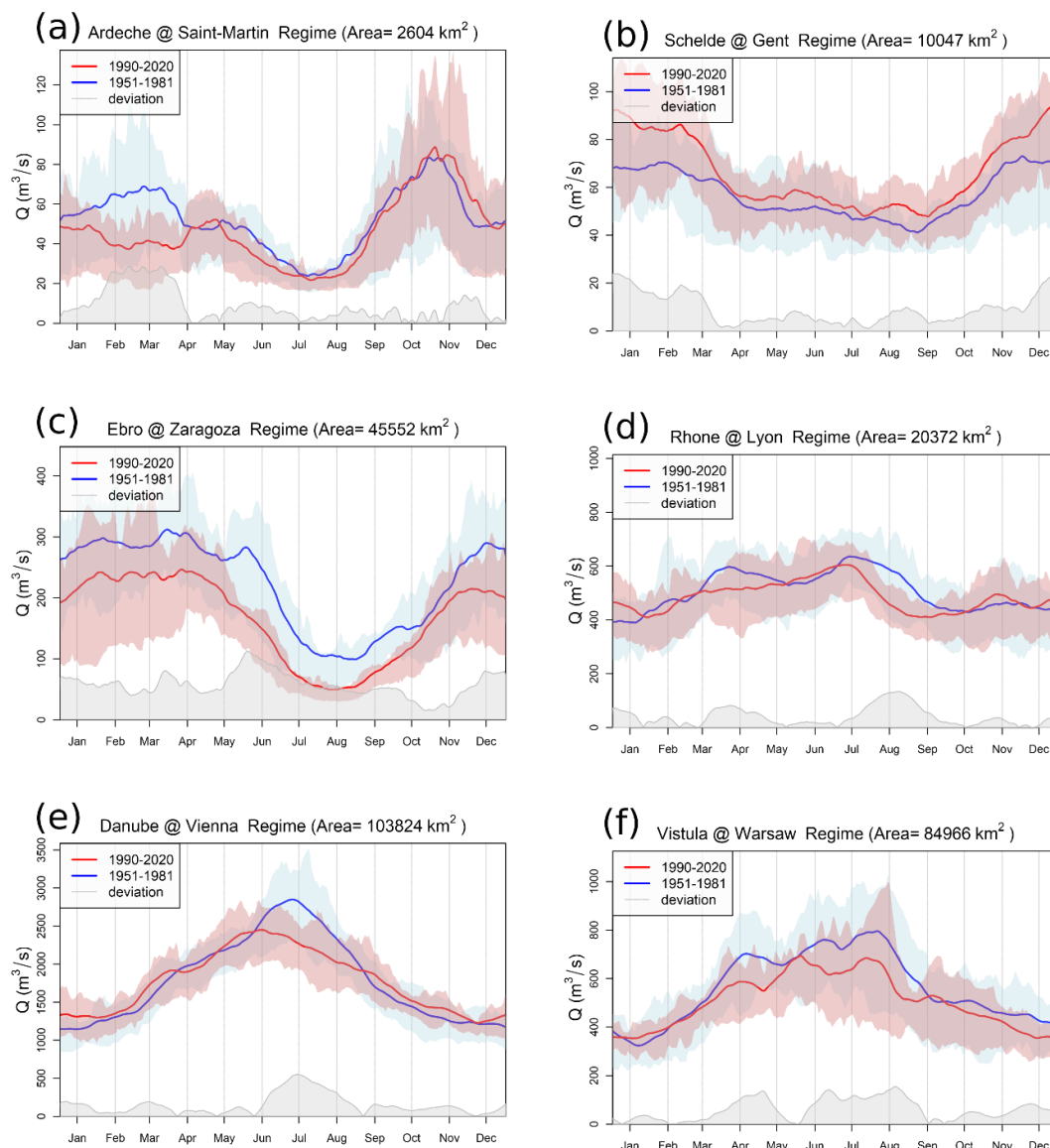
Usage notes

665 ~~The HERA datasets~~ brings together ~~developments from its inputs~~ several improvements (climate, scale, socio-economic dynamics) to ~~the hydrological modelling that have been described~~ better simulate river discharge in ~~Section 2 and quantified in Section 3.1~~ catchments of Europe over the past 70 years. Despite covering still ~~being~~ a relatively short period of time compared to human history on earth, ~~the 70 years of homogeneous modelled river flow provided by HERA captures the most~~ these 70 years ~~capture a very~~ intense period of climate and socioeconomic change, often called the Anthropocene, and offers multiple research opportunities:

- Assessment of long-term trends in European river regimes
- ~~Provision of~~ Provide benchmark data for “data poor” areas
- ~~Generation of~~ Generate catalogues of flood and drought events
- 675 • Identification of spatial and temporal correlations between European catchments
- Identification of changes in hydrological extremes characteristics (frequency, magnitude, timing)
- Combination with other data products for compound hazard analysis
- ~~Provision of~~ Provide scenarios for flood inundation simulations

680 In this section, we briefly present a ~~simple~~ possible usage of the data, addressing changes in regime for diverse rivers across Europe (**Figure 10**).





685

Figure 10: Changes in hydrological regimes flow regime between the first (1951-1981 (blue) and the last (1990-2020) 30-years periods (red) for six diverse European rivers: (a) Ardèche, (b) Schelde, (c) Ebro, (d) Rhone, (e) Danube and (f) Vistula. The regime is computed here as the 30-day moving average. Shaded coloured areas represent the IQR of discharge for every day of the year. The grey shaded area represents the absolute difference between the two regimes corresponding to different periods.

690

Figure 10 displays hydrological regimes, here represented as the mean of a 30-days' day's average moving window over a given period, for six European rivers. These rivers differs in terms of hydrological regimes, with three main regimes represented:

695

- Mediterranean pluvial regime for the Ardèche (a), with its recognisable high flows in autumn.
- Pluvial or oceanic regime for the Schelde in Ghent (b) and the Ebro in Zaragoza (c)
- Nival regime for the upper Rhone in Lyon (d), the Danube in Vienna (e) and the Vistula in Warsaw (f).

These six rivers also vary in terms catchment area, geographic location (France, Austria, Poland, Belgium, Spain) ~~climates present in their upstream areas~~, climate (Mediterranean, Continental,

Oceanic, Alpine) and geomorphiegeomorphological conditions. ~~In Figure 10, two regimes are displayed for~~ For each river, ~~in blue for the period flow regime for 1951 – 1981 (in blue, first 30 years without 1950, which is impacted by the spin-up of LISFLOOD (LISFLOOD-OS online documentation, 2023), HERA) and 1990 – 2020 (in red for the second for the, last 30 years of the simulation, 1980 – 2020HERA) are shown.~~ By comparing the two regimes, one can observe diverging patterns of changes among these rivers. For ~~instancethe two pluvial rivers,~~ the Schelde and the Ebro, ~~(Figure 10.b-c),~~ both pluvial rivers ~~see, we observe~~ opposite patterns of change, the Schelde ~~seesaw~~ an increase of its average discharge throughout the year, while the Ebro ~~has experienced~~ a ~~constant water deficit downward shift in regime.~~ For the upper Rhone and Danube, ~~(Figure 11.d-e),~~ which are influenced by snowmelt in their upper catchments, we see lower and earlier flow peaks in spring and summer. The Vistula ~~sees(Figure 11.f) saw~~ an overall increase in flow throughout the year. Finally, the Ardèche ~~(Figure 11.a) has seen~~ reduced flow throughout the year, with a notable decrease in ~~late winter, which can be associated to the reduction of snowfall in the Massif Central where the Ardèche has its up waters (François et al., 2023).~~ The timing of the autumn peak ~~seemsseem~~ to have slightly shifted towards earlier dates, ~~a feature which was also unravelled inin agreement with~~ a recent study on trends in Mediterranean floods (Tramblay et al., 2023).

~~Previous studies, focusing on different metrics and periods already highlighted comparable diverging patterns between different European regions (Peña-Angulo et al., 2022; Stahl et al., 2012; Blöschl et al., 2019a).~~

Discussion

Recent developments in diverse ~~scientific~~ fields, including climate ~~modelling, hydrological modelling and, hydrology,~~ remote sensing ~~and computational sciences,~~ have made the generation of high-resolution reanalysis products possible. ~~As a result, the HERA dataset (Aerts et al., 2022; Hanasaki et al., 2022; Hoch et al., 2023).~~ In this context, HERA brings discharge data for all European rivers with upstream area larger than 100 km²: ~~for the period 1951-2020.~~ With its refined spatial and temporal resolution, HERA ~~captures dynamiesrepresents hydrological processes in extremes events (floods and drought), reveals spatial heterogeneities and simulates anthropogenic water useEurope~~ with more ~~accuracydetail~~ than ~~any otherprevious publicly available~~ hydrological reanalysis products (Harrigan et al., 2020; Schellekens et al., 2017). Calibrating hydrological models can significantly improve river flow simulation (Beck et al., 2017; Kauffeldt et al., 2016). ~~AroundParameters in~~ 93.5% of the HERA ~~domain received specific calibration parameters through thewere adjusted during a~~ calibration process (Section 2.1.2) or parameter regionalization (Beck et al., 2016). This is a very high calibration coverage

for a GHM, which are not systematically calibrated (Beck et al., 2017), that can be explained by the relatively high coverage in river gauging stations in Europe.

735 It is difficult to compare HERA with ~~two other~~ recent hydrological ~~reanalysis;reanalyses~~ such as GLOFAS-ERA5 (Harrigan et al., 2020) and GRFR (Yang et al., 2021), for several reasons: ~~the two~~ ~~mentioned dataset are~~ (i) spatial coverage (global, ~~have larger vs continental~~), (ii) spatial resolution (~~respectively 0.25° and 0.05°~~), ~~shorter, 1'~~, (iii) temporal coverage (iv) dynamic vs static socioeconomic conditions. A comparison with the European-scale hydrological simulation with the mHM model (EUmHM) (see **Supplementary Material Figure S3-S6**) shows that HERA generally
740 outperforms the EUmHM run in terms of KGE' (Figure S4) but both models exhibit strengths and weaknesses spatially (**Figure S5**) and ~~do not account for anthropogenic land~~ in terms of the components of KGE' (**Figure S6**). Differences in performances between the HERA and ~~water use changes~~. EUmHM run can be attributed to the many different features in the two runs, such as meteorological forcing, resolution, calibration, and flow routing within the hydrological model. Conversely, HERA shares a
745 great ~~amount number~~ of features with the EFAS v5.0 reanalysis (Decremer et al., 2023), with comparable ~~performances~~. performance (not shown here). Nonetheless, EFAS v5.0 only covers the period 1990 – 2022 and assumes static socioeconomic conditions (land use, water abstraction, reservoirs).

750 Similarly to other aforementioned hydrological ~~reanalysis;reanalyses~~, HERA exhibits reduced performance in cold and semi-arid catchments. This can be related to ~~model errors~~. deficiencies in ~~modelling the representation of~~ snow processes within OS LISFLOOD or the underestimation of precipitation ~~in~~ at northern latitudes (Beck et al., 2017, 2020). Semi-arid environments are notoriously challenging areas for hydrological models due to ~~their strong interannual variability in~~ the highly non-linear rainfall-runoff response and lower precipitation ~~and runoff data quality~~ (Cantoni et al., 2022). GHMs, ~~including LISFLOOD~~, tend to poorly represent runoff in small-to-medium size catchments (10-
755 ~~10-000~~ 10-1000 km², 1000 km²) (Harrigan et al., 2020; Sood and Smakhtin, 2015), and nearly 90% of the catchments used in the validation of HERA (**Section 3.1**) are small-to-medium size catchments. The drop in performance with smaller catchment area in HERA remains, however, moderate compared to
760 the GLOFAS-ERA5 global hydrological reanalysis (Harrigan et al., 2020). The presence of reservoirs also ~~has an impact on reanalysis performances~~. influences the performance of reanalyses. While including reservoirs in the hydrological modelling has a positive impact on LISFLOOD performances. model performance (Zajac et al., 2017), there is still a high level of uncertainty ~~remains~~ ~~on~~ regarding the operating rules ~~specific to of~~ each reservoir ~~or operators~~. Moreover, the 1422 reservoirs
765 used to generate HERA most likely ~~only~~ represent just a fraction (~~mainly the largest ones~~), of all operational reservoirs ~~currently in operation~~ in the modelled domain (Speckhann et al., 2021).

HERA is generated through hydrological modelling, which brings a suite of uncertainties. ~~Uncertainties in hydrological modelling that~~ can be divided into four categories: (i) model inputs, (ii) model structure, (iii) parameter values and (iv) ~~observed data observations~~. It remains challenging to quantify these uncertainties, however, the quality of inputs, and more in particular climate inputs is often referred to as an important factor of uncertainty (Beck et al., 2017; Sood and Smakhtin, 2015). The improvement of overall modelling ~~performances performance~~ through time ~~highlighted in Figure 7.a~~ could therefore be related to improving climate inputs. ~~Indeed, the quality of climate reanalysis are influenced by the availability of, as~~ observations, ~~which~~ in ERA5-land become ~~sparser and more sparse and~~ inhomogeneous as we go back further in time (Hersbach et al., 2020; Muñoz-Sabater et al., 2021). Despite efforts in bias ~~correcting correction~~ and downscaling ~~our of the~~ climate ~~inputs input~~, it seems that on average, HERA slightly underestimates river discharges, with a more pronounced bias for high flows. ~~These biases This~~ can be related to an underestimation of precipitation in ~~our the~~ climate inputs, in particular for extreme events (McClean et al., 2023; Mahto and Mishra, 2019). ~~It has also been shown that uncertainties in precipitations can result in even higher uncertainties in runoff) and~~ in (semi-)arid catchments (Beck et al., 2016; Sood and Smakhtin, 2015). ~~Uncertainties inherent to Model structure can also play an important role, as shown in Figure S6, where EUmHM is the best model structures have long been overshadowed (Beck et al., 2017). Nonetheless, their~~ terms of correlation while HERA exhibits smaller bias ratio. This can be the result of different choices made in the main equation behind ~~the two models. The~~ large impact of model selection on streamflow and trend estimates is now increasingly acknowledged (Karlsson et al., 2016; Clark et al., 2016). ~~The method and parameters used for calibration further affects the uncertainty, with higher performances for stations used in the calibration process (Figure .8.d).~~ Other uncertainties ~~ear can~~ arise from surface field maps (Section 2.3) and ~~calibration parameters, even if these latter are reduced by the model calibration procedure. Ultimately, uncertainties remain even in the data we consider as “ground truth”: flow measurements. These uncertainties are related to the way measuring of river discharge is measured discharges~~ (instruments and rating curves). ~~And with With~~ sparser gauging and more complex hydraulic conditions for high and low flows, uncertainty rises (Despax, 2016).

Data availability

~~We make available the~~The HERA hydrological reanalysis ~~along with it and its~~ climate and dynamic socioeconomic inputs ~~through are available via~~ the JRC data catalogue ~~at~~ <http://data.europa.eu/89h/a605a675-9444-4017-8b34-d66be5b18c95> (Tilloy et al., 2024). **Table 1** provides a brief description of the dataset and **Table 2** gives a general overview of the content of the dataset.

Table 1: Description of the HERA dataset

DATASET DESCRIPTION	
Data type	Gridded
Projection	WGS 1984 – EPSG 4326
Spatial coverage	EU27, UK, Switzerland, Iceland, Norway, Serbia, Montenegro, Bosnia-Herzegovina, Kosovo, North Macedonia, Albania
Temporal coverage	03-01-1950 <u>01-1951</u> to 31-12-2020
Temporal resolution	Six-hourly data
File format	netcdf

~~We want to stress here that even if the hydrological reanalysis starts on January 3rd 1950, discharge values in the first months may be inaccurate due the lower zone's spin up (Burek *et al.*, 2013), especially in dry catchments. We therefore do not recommend to use data for the beginning of 1950.~~

The dataset consists of three distinct folders that are described here and in **Table 2**:

- Climate inputs: folder containing the climate ~~forcings use to run~~forcing for the LISFLOOD hydrological model. Out of the five variables provided, three are at daily temporal resolution, potential evapotranspiration, potential evaporation and potential evaporation from bare soil (obtain with LISVAP, LISVAP online documentation, 2023), while two have a six-hourly time step, precipitation and temperature. The spatial resolution of the climate inputs is 1'. The files are in netcdf format with one file per year per variable for a total of 355 files (2.3 TB of data).
- Socioeconomic inputs: folder containing the dynamic surface fields maps (**Section 2.3**), divided into three categories: land use, reservoirs and water demand. The land use subfolder contains 426 yearly files (4.6 GB) of land use fraction maps for each six land use classes. The reservoir subfolder hosts 71 yearly files (3.6 GB) of reservoir location and identifier, ~~reservoirs.~~ Reservoirs are added/discarded from the simulation every year according to their construction/destruction data. Finally, the water demand subfolders ~~contains~~contain four files (3.9 GB) representing water demand for the considered sectors (**Section 2.3.3**). Each file contains monthly maps of water abstraction for a given sector. All socioeconomic inputs are provided in the netcdf format.
- River discharge: this folder contains ~~the flagship of the present dataset, yearly~~ river discharge netcdf files for each year at six-hourly time step for all European ~~river.~~ river. ~~The initial output of LISFLOOD was filtered to retain solely~~ rivers with an upstream area greater than 100 km². ~~This results in continuous streamflow estimates for 282 521 river pixels and significantly reduces data size~~ (2.3 GB per file, 166 GB total).

830 All data ~~from this dataset~~ share the same projection (WGS 84) grid and spatial resolution (1'). Static surface fields maps were directly retrieved from the [OS LISFLOOD](#) static and parameter maps for Europe ([2024](#)) dataset ([Choulga et al., 2023b](#)), which were developed in the context of the new EFAS deployment (Decremer et al., 2023). It is important to note that HERA simulates discharge on a slightly smaller domain than the original EFAS domain, the mask used for HERA is also provided in the dataset.

835 **Table 2: List of inputs and outputs of LISFLOOD provided in the HERA database (link here).**

Subfolder	File	Resolutions	Variable/content	Unit
	area_hera_01min.nc	1'	<i>mask of the hera domain</i>	
climate_inputs/ e0	e0_yyyy.nc	1', daily	<i>potential evaporation computed with lisvap from downscaled and bias-corrected actual vapour pressure, solar radiations, min/max daily temperature and 10m wind speed.com</i>	mm.d ⁻¹
climate_inputs/ et0	et0_yyyy.nc	1', daily	<i>potential evapotranspiration computed with lisvap from downscaled and bias-corrected actual vapour pressure, solar radiations, min/max daily temperature and 10m wind speed.com</i>	mm.d ⁻¹
climate_inputs/ es0	es_yyyy.nc	1', daily	<i>potential evaporation from bare soil computed with lisvap from downscaled and bias-corrected actual vapour pressure, solar radiations, min/max daily temperature and 10m wind speed.</i>	mm.d ⁻¹
climate_inputs/ pr6	pr6_yyyy.nc	1', six- hourly	<i>downscaled and bias-corrected six-hourly precipitation</i>	mm.d ⁻¹
climate_inputs/ tp6	ta6_yyyy.nc	1', six- hourly	<i>downscaled and bias-corrected six-hourly average temperature</i>	°c
socioeconomic_ maps/landuse	fracforest_european _01min_yyyy.nc	1', yearly	<i>fraction of pixel area covered by evergreen and deciduous needle leaf and broad leaf tree areas</i>	
socioeconomic_ maps/landuse	fracsealed_europea n_01min_yyyy.nc	1', yearly	<i>fraction of pixel area covered by urban areas, characterizing the human impact on the environment</i>	
socioeconomic_ maps/landuse	fracirrigated_europ ean_01min_yyyy.nc	1', yearly	<i>fraction of pixel area covered by irrigated areas of all possible crops excluding rice</i>	
socioeconomic_ maps/landuse	fracwater_european _01min_yyyy.nc	1', yearly	<i>fraction of pixel area covered by rivers, freshwater and saline lakes, ponds and other permanent water bodies over the continents</i>	

socioeconomic_ maps/landuse	fracrice_european_01min_yyyy.nc	1', yearly	<i>fraction of pixel area covered by irrigated areas of rice</i>	
socioeconomic_ maps/landuse	fracother_european_01min_yyyy	1', yearly	<i>fraction of pixel area covered by agricultural areas, non-forested natural area, pervious surface of urban areas</i>	
socioeconomic_ maps/reservoirs	res_european_01min_yyyy.nc	1', yearly	<i>location and identifier of each reservoir</i>	
socioeconomic_ maps/water_demand	dom_1950_2020.nc	1', monthly	<i>daily supply of water volume for indoor and outdoor household purposes and for all the uses that are connected to the municipal system (e.g., water used by shops, schools, and public buildings)</i>	mm.d ⁻¹
socioeconomic_ maps/water_demand	ene_1950_2020.nc	1', monthly	<i>daily supply of water volume for fabricating, processing, washing and sanitation, cooling or transporting a product, incorporating water into a product</i>	mm.d ⁻¹
socioeconomic_ maps/water_demand	ind_1950_2020.nc	1', monthly	<i>daily supply of water volume for the cooling of thermoelectric and nuclear power plant</i>	mm.d ⁻¹
socioeconomic_ maps/water_demand	liv_1950_2020.nc	1', monthly	<i>daily supply of water volume for domestic animal need</i>	mm.d ⁻¹
river_discharge	dis.herayyyy.nc	1', six-hourly	<i>river discharge for river pixels with upstream area > 100km².</i>	m ³ .s ⁻¹

Conclusion

Despite the limitations discussed above, HERA ~~successfully delivers~~represents a state-of-the-art, high-resolution, long-term hydrological reanalysis for Europe in the form of homogeneous river flow data generated with the OS LISFLOOD model. ~~While covering a much longer period than the EFAS v5.0 reanalysis, HERA benefits from the development and calibration associated with this latter, which represent steps forward compared to previous EFAS hydrological reanalysis.~~ To our knowledge, no other publicly available hydrological reanalysis currently provides discharge data for Europe at similar scales with a similar temporal and spatiotemporal coverage. ~~Due to its extensive period, the datasets is particularly suited for the assessment of long term trends of several hydrological signatures. The unprecedented spatial resolution allows for a robust analysis of small to medium catchments at continental scale. One of the main objectives of HERA is to advance the reproduction of extreme events,~~

850 notably by the mean of the sub-daily temporal resolution and bias corrected climate input. On average,
both magnitude and seasonality of extremes are well simulated, even if more work is needed to fully
855 assess HERA performances in reproducing extremes, in particular for high flows. for Europe. The
inclusion of dynamic socioeconomic conditions ~~further~~ provides a more realistic reanalysis of river
flows in heavily managed European catchments. The increased spatial resolution improves the
performance due to a better representation of hydrological processes and inputs required to simulate
them, including the river network (Hoch et al., 2023; Thober et al., 2019). HERA advances the
860 reanalysis of extreme hydrological events, notably by the sub-daily temporal resolution and high-
resolution bias corrected climate input. The magnitude and seasonality of extremes are fairly
reproduced, even if biases exist in some regions (e.g., central Poland, southern Spain). The dataset
covers 70 years and is therefore suited for the analysis of long-term trends of several hydrological
signatures. The modelling framework developed here further forms a basis for creating alternative
(counterfactual) time series of river discharges where climatic or socioeconomic conditions can be kept
static ~~rather than dynamic~~, enabling the attribution of changes in hydrological regimes across Europe
(Kreibich et al., 2019; Sauer et al., 2021; Scussolini et al., 2023).

Code availability

865 ~~The lisflood model is open source and available on github along with a set of auxiliary tools~~
~~(<https://github.com/ec-jrc/lisflood-code>). A sample of the settings file used to generate HERA discharge~~
~~data with lisflood is provided along with the Python and R codes used to validate the simulation and~~
~~generate the figure displayed in this manuscript are available on github~~
~~(<https://github.com/Alovis/HERA>)~~

870 **Supplement**

Author contribution

Alois Tilloy: conceptualization, data curation, formal analysis, software, writing – original draft preparation. **Dominik Paprotny**: conceptualization, methodology, formal analysis, writing – original draft preparation. **Stefania Grimaldi**: methodology, software, supervision. **Cinzia Mazzetti**: methodology, software. **Goncalo Gomes**: software. **Alessandra Bianchi**: visualization. **Stefan Lange**: conceptualization, methodology, writing – reviewing and editing. **Hylke Beck**: conceptualization, methodology, writing – reviewing and editing. **Luc Feyen**: conceptualization, methodology, supervision, writing – reviewing and editing.

880

Acknowledgments

Competing interests

The authors declare that they have no conflict of interest.

885

Financial support

~~Dominik Paprotny was supported by the German Research Foundation (DFG) through project~~
~~“Decomposition of flood losses by environmental and economic drivers” (FloodDrivers), grant no.~~
~~449175973.~~

890 **References**

[Aerts, J. P. M., Hut, R. W., Van De Giesen, N. C., Drost, N., Van Verseveld, W. J., Weerts, A. H., and Hazenberg, P.: Large-sample assessment of varying spatial resolution on the streamflow estimates of the wflow sbm hydrological model, Hydrol. Earth Syst. Sci., 26, 4407–4430, <https://doi.org/10.5194/hess-26-4407-2022>, 2022.](https://doi.org/10.5194/hess-26-4407-2022)

895 Alfieri, L., Lorini, V., Hirpa, F. A., Harrigan, S., Zsoter, E., Prudhomme, C., and Salamon, P.: A global streamflow reanalysis for 1980–2018, *Journal of Hydrology* X, 6, 100049, <https://doi.org/10.1016/j.hydroa.2019.100049>, 2020.

900 Allen, R. G., Pereira, L. S., Raes, D., and Smith, M.: FAO Irrigation and Drainage Paper, https://www.researchgate.net/publication/284300773_FAO_Irrigation_and_drainage_paper_No_56, last access: 11 January 2024, 1998.

Batista e Silva, F., Lavallo, C., and Koomen, E.: A procedure to obtain a refined European land use/cover map, *Journal of Land Use Science*, 8, 255–283, <https://doi.org/10.1080/1747423X.2012.667450>, 2013.

905 Beck, H. E., van Dijk, A. I. J. M., de Roo, A., Miralles, D. G., McVicar, T. R., Schellekens, J., and Bruijnzeel, L. A.: Global-scale regionalization of hydrologic model parameters, *Water Resources Research*, 52, 3599–3622, <https://doi.org/10.1002/2015WR018247>, 2016.

Beck, H. E., van Dijk, A. I. J. M., de Roo, A., Dutra, E., Fink, G., Orth, R., and Schellekens, J.: Global evaluation of runoff from 10 state-of-the-art hydrological models, *Hydrology and Earth System Sciences*, 21, 2881–2903, <https://doi.org/10.5194/hess-21-2881-2017>, 2017.

910 Beck, H. E., [Wood, E. F., Mcvicar, T. R., Zambrano-Bigiarini, M., Alvarez-Garretón, C., Baez-Villanueva, O. M., Sheffield, J., and Karger, D. N.: Bias Correction of Global High-Resolution Precipitation Climatologies Using Streamflow Observations from 9372 Catchments, *JOURNAL OF CLIMATE*, 33, 2020.](#)

915 [Beck, H. E.,](#) Dijk, A. I. J. M. van, Larraondo, P. R., McVicar, T. R., Pan, M., Dutra, E., and Miralles, D. G.: MSWX: Global 3-Hourly 0.1° Bias-Corrected Meteorological Data Including Near-Real-Time Updates and Forecast Ensembles, *Bulletin of the American Meteorological Society*, 103, E710–E732, <https://doi.org/10.1175/BAMS-D-21-0145.1>, 2022.

920 Berghuijs, W. R., Harrigan, S., Molnar, P., Slater, L. J., and Kirchner, J. W.: The Relative Importance of Different Flood-Generating Mechanisms Across Europe, *Water Resources Research*, 55, 4582–4593, <https://doi.org/10.1029/2019WR024841>, 2019.

925 Blöschl, G., Hall, J., Viglione, A., Perdigão, R. A. P., Parajka, J., Merz, B., Lun, D., Arheimer, B., Aronica, G. T., Bilibashi, A., Boháč, M., Bonacci, O., Borga, M., Čanjevac, I., Castellarin, A., Chirico, G. B., Claps, P., Frolova, N., Ganora, D., Gorbachova, L., Gül, A., Hannaford, J., Harrigan, S., Kireeva, M., Kiss, A., Kjeldsen, T. R., Kohnová, S., Koskela, J. J., Ledvinka, O., Macdonald, N., Mavrova-Guirguinova, M., Mediero, L., Merz, R., Molnar, P., Montanari, A., Murphy, C., Osuch, M., Ovcharuk, V., Radevski, I., Salinas, J. L., Sauquet, E., Šraj, M., Szolgay, J., Volpi, E., Wilson, D., Zaimi, K., and Živković, N.: Changing climate both increases and decreases European river floods, *Nature*, 573, 108–111, <https://doi.org/10.1038/s41586-019-1495-6>, 2019a.

930 Blöschl, G., Bierkens, M. F. P., Chambel, A., Cudennec, C., Destouni, G., Fiori, A., Kirchner, J. W., McDonnell, J. J., Savenije, H. H. G., Sivapalan, M., Stumpp, C., Toth, E., Volpi, E., Carr, G., Lupton, C., Salinas, J., Széles, B., Viglione, A., Aksoy, H., Allen, S. T., Amin, A., Andréassian, V., Arheimer, B., Aryal, S. K., Baker, V., Bardsley, E., Barendrecht, M. H., Bartosova, A., Batelaan, O., Berghuijs, W. R., Beven, K., Blume, T., Bogaard, T., Borges De Amorim, P., Böttcher, M. E., Boulet, G., Breinl, K., Brilly, M., Brocca, L., Buytaert, W., Castellarin, A., Castelletti, A., Chen, X., Chen, Y., Chen, Y., Chiffard, P., Claps, P., Clark, M. P., Collins, A. L., [Croke, B., Dathe, A., David, P. C., De Barros, F. P. J., De Rooij, G., Di Baldassarre, G., Driscoll, J. M., Duethmann, D., Dwivedi, R., Eris, E., Farmer, W. H., Feiccabrino, J., Ferguson, G., Ferrari, E., Ferraris, S., Fersch, B., Finger, D., Foglia, L., Fowler, K., Gartsman, B., Gascoin, S., Gaume, E., Gelfan, A., Geris, J., Gharari, S., Gleeson, T., Glendell, M., Gonzalez Bevacqua, A., González-Dugo, M. P., Grimaldi, S., Gupta, A. B., Guse, B., Han, D., Hannah, D., Harpold, A., Haun, S., Heal, K., Helfricht, K., Herrnegger, M., Hipsey, M., Hlaváčiková, H.,](#)

[Hohmann, C., Holko, L., Hopkinson, C., Hrachowitz, M., Illangasekare, T. H., Inam, A., Innocente, C., Istanbuluoglu, E., Jarihani, B., et al.:](https://doi.org/10.1080/02626667.2019.1620507) Twenty-three unsolved problems in hydrology (UPH) – a community perspective, *Hydrological Sciences Journal*, 64, 1141–1158, <https://doi.org/10.1080/02626667.2019.1620507>, 2019b.

945 Brönnimann, S., Allan, R., Atkinson, C., Buizza, R., Bulygina, O., Dahlgren, P., Dee, D., Dunn, R.,
Gomes, P., John, V. O., Jourdain, S., Haimberger, L., ~~Hersbach~~Hersbach, H., Kennedy, J., Poli, P.,
Pulliainen, J., Rayner, N., Saunders, R., Schulz, J., Sterin, A., Stickler, A., Titchner, H., Valente, M. A.,
Ventura, C., and Wilkinson, C.: Observations for ~~reanalyses~~, *B. Am. Meteorol. Soc.*, 99,
950 ~~1851–1866~~[Reanalyses](https://doi.org/10.1175/BAMS-D-17-0229.1), *Bulletin of the American Meteorological Society*, 99, 1851–1866,
<https://doi.org/10.1175/BAMS-D-17-0229.1>, 2018.

Brunner, M. I.: Reservoir regulation affects droughts and floods at local and regional scales, *Environ. Res. Lett.*, 16, 124016, <https://doi.org/10.1088/1748-9326/ac36f6>, 2021.

Brunner, M. I., ~~Slater, L., Tallaksen, L. M., and Clark, M.:~~ [Challenges in modeling and predicting floods and droughts: A review](https://doi.org/10.1002/wat2.1520), *WIREs Water*, 8, <https://doi.org/10.1002/wat2.1520>, 2021a.

955 ~~Brunner, M. I.,~~ Melsen, L. A., Wood, A. W., Rakovec, O., Mizukami, N., Knoben, W. J. M., and Clark,
M. P.: Flood spatial coherence, triggers, and performance in hydrological simulations: large-sample
evaluation of four streamflow-calibrated models, *Hydrology and Earth System Sciences*, 25, 105–119,
<https://doi.org/10.5194/hess-25-105-2021>, ~~2021b~~2021.

960 Burek, P., van der Knijff, J., and De Roo, A.: LISFLOOD - Distributed Water Balance and Flood
Simulation Model - Revised User Manual 2013,
~~<https://publications.jrc.ec.europa.eu/repository/handle/JRC78917>, last access: 12 January 2024,~~
~~2013.2013.~~

965 Calvin, K., Patel, P., Clarke, L., Asrar, G., Bond-Lamberty, B., Cui, R. Y., Di Vittorio, A., Dorheim,
K., Edmonds, J., Hartin, C., Hejazi, M., Horowitz, R., Iyer, G., Kyle, P., Kim, S., Link, R., McJeon, H.,
Smith, S. J., Snyder, A., Waldhoff, S., and Wise, M.: GCAM v5.1: representing the linkages between
energy, water, land, climate, and economic systems, *Geoscientific Model Development*, 12, 677–698,
<https://doi.org/10.5194/gmd-12-677-2019>, 2019.

970 Cammalleri, C., Vogt, J., and Salamon, P.: Development of an operational low-flow index for
hydrological drought monitoring over Europe, *Hydrological Sciences Journal*, 62, 346–358,
<https://doi.org/10.1080/02626667.2016.1240869>, 2017.

Cammalleri, C., Gustavo Naumann, Naumann, G., Mentaschi, L., Bisselink, B., Gelati, E., de Roo, A.,
and Feyen, L.: Diverging hydrological drought traits over Europe with global warming, *Hydrology and
Earth System Sciences Discussions*, 24, 5919–5935, <https://doi.org/10.5194/hess-2020-93>, 2020a.

975 Cammalleri, C., P. Barbosa, Barbosa, P., Barbosa, P., and Vogt, J.: Evaluating simulated daily discharge
for operational hydrological drought monitoring in the Global Drought Observatory (GDO),
Hydrological Sciences Journal-journal Des Sciences Hydrologiques, 65, 1316–1325,
<https://doi.org/10.1080/02626667.2020.1747623>, 2020b.

980 [Cannon, A. J.: Multivariate quantile mapping bias correction: an N-dimensional probability density
function transform for climate model simulations of multiple variables](https://doi.org/10.1007/s00382-017-3580-6), *Clim Dyn*, 50, 31–49,
<https://doi.org/10.1007/s00382-017-3580-6>, 2018.

Cantoni, E., Tramblay, Y., Grimaldi, S., Salamon, P., Dakhlaoui, H., Dezetter, A., and Thiemi, V.:
Hydrological performance of the ERA5 reanalysis for flood modeling in Tunisia with the LISFLOOD
and GR4J models, *Journal of Hydrology: Regional Studies*, 42, 101169,
<https://doi.org/10.1016/j.ejrh.2022.101169>, 2022.

- 985 ~~CEMS-Flood online documentation: <https://confluence.ecmwf.int/display/CEMS/CEMS-Flood>, last access: 14 December 2023.~~
- Choulga, M., Moschini, F., Mazzetti, C., Grimaldi, S., Disperati, J., Beck, H., Salamon, P., and Prudhomme, C.: Technical note: Surface fields for global environmental modelling, <https://doi.org/10.5194/egusphere-2023-1306>, 21 August ~~2023a~~2023.
- 990 ~~Choulga, M. M., Beck, H., Moschini, F., Mazzetti, C., Grimaldi, S., Disperati, J., Salamon, P., and Prudhomme, C.: LISFLOOD static and parameter maps for Europe, [dataset] Joint Research Centre Data Catalogue, 2023b.~~
- Clark, M. P., Wilby, R. L., Gutmann, E. D., Vano, J. A., Gangopadhyay, S., Wood, A. W., Fowler, H. J., Prudhomme, C., Arnold, J. R., and Brekke, L. D.: Characterizing Uncertainty of the Hydrologic Impacts of Climate Change, *Curr Clim Change Rep*, 2, 55–64, <https://doi.org/10.1007/s40641-016-0034-x>, 2016.
- 995 ~~CEMS-Flood online documentation: <https://confluence.ecmwf.int/display/CEMS/CEMS-Flood>, last access: 14 December 2023.~~
- 1000 Copernicus: Copernicus Global Land Service - LAI, [dataset] <https://land.copernicus.eu/global/products/lai>, [dataset], 2021.
- Decremer, D., Mazzetti, C., Carton, C., Gomes, G., Russo, C., Ramos, A., Grimaldi, S., Disperati, J., Ziese, M., Garcia Sanchez, R., Jacobson, T., Salamon, P., and Prudhomme, C.: EFAS v5.0 hydrological reanalysis, [dataset] Joint Research Centre Data Catalogue, [dataset], 2023.
- 1005 Despax, A.: Incertitude des mesures de débit des cours d'eau au courantomètre. Amélioration des méthodes analytiques et apports des essais interlaboratoires, These de doctorat, Université Grenoble Alpes (ComUE), 2016.
- 1010 ~~De Roo, A., Odijk, M., Schmuck, G., Koster, E., and Lucieer, A.: Assessing the effects of land use changes on floods in the meuse and oder catchment, *Physics and Chemistry of the Earth, Part B: Hydrology, Oceans and Atmosphere*, 26, 593–599, [https://doi.org/10.1016/S1464-1909\(01\)00054-5](https://doi.org/10.1016/S1464-1909(01)00054-5), 2001.~~
- ~~Dottori, F., Alfieri, L., Bianchi, A., Skoien, J., and Salamon, P.: A new dataset of river flood hazard maps for Europe and the Mediterranean Basin, *Earth System Science Data*, 14, 1549–1569, <https://doi.org/10.5194/essd-14-1549-2022>, 2022.~~
- 1015 Donat, M. G., Sillmann, J., Wild, S., Alexander, L. V., Lippmann, T., and Zwiers, F. W.: Consistency of ~~temperature~~Temperature and ~~precipitation extremes~~Precipitation Extremes across ~~various global gridded in situ~~Various Global Gridded In Situ and ~~reanalysis datasets~~Reanalysis Datasets, *J. Climate*, 27, 5019–5035, <https://doi.org/10.1175/JCLI-D-13-00405.1>, 2014.
- 1020 Ekolu, J., Dieppois, B., Sidibe, M., Eden, J. M., Trambly, Y., Villarini, G., Peña-Angulo, D., Mahé, G., Paturel, J.-E., Onyutha, C., and van de Wiel, M.: Long-term variability in hydrological droughts and floods in sub-Saharan Africa: New perspectives from a 65-year daily streamflow dataset, *Journal of Hydrology*, 613, 128359, <https://doi.org/10.1016/j.jhydrol.2022.128359>, 2022.
- ~~LISFLOOD OS online documentation: <https://ec-jrc.github.io/lisflood/>, last access: 15 December 2023.~~
- ~~LISVAP online documentation: <https://ec-jrc.github.io/lisflood-lisvap/>, last access: 15 December 2023.~~
- ~~FAO: AQUASTAT, [dataset] <https://www.fao.org/aquastat/en/>, 2023.~~

- 1025 Feyen, L. and Dankers, R.: Impact of global warming on streamflow drought in Europe, *J. Geophys. Res.*, 114, D17116, <https://doi.org/10.1029/2008JD011438>, 2009.
- Florczyk, A. J., Corbane, C., Ehrlich, D., Freire, S., Kemper, T., Maffenini, L., Melchiorri, M., Pesaresi, M., Politis, P., Schiavina, M., Sabo, F., and Zanchetta, L.: GHSL Data Package 2019 - Technical report by the Joint Research Centre (JRC), European Union, 38 pp., <https://doi.org/10.2760/0726>, 2019.
- 1030 [Food and Agriculture Organisation: AQUASTAT](https://www.fao.org/aquastat/en/), , <https://www.fao.org/aquastat/en/>, 2023.
- [Fortin, F.-A., De Rainville, F.-M., Gardner, M.-A., Parizeau, M., and Gagné, C.: DEAP: Evolutionary Algorithms Made Easy, *Journal of Machine Learning Research*, 13, 2171–2175, 2012.](https://doi.org/10.2760/0726)
- [François, H., Samacoïts, R., Bird, D. N., Köberl, J., Pretenthaler, F., and Morin, S.: Climate change exacerbates snow-water-energy challenges for European ski tourism, *Nat. Clim. Chang.*, 13, 935–942, <https://doi.org/10.1038/s41558-023-01759-5>, 2023.](https://doi.org/10.1038/s41558-023-01759-5)
- 1035 Frieler, K., Volkholz, J., Lange, S., Schewe, J., Mengel, M., del Rocío Rivas López, M., Otto, C., Reyer, C. P. O., Karger, D. N., Malle, J. T., Treu, S., Menz, C., Blanchard, J. L., Harrison, C. S., Petrik, C. M., Eddy, T. D., Ortega-Cisneros, K., Novaglio, C., Rousseau, Y., Watson, R. A., Stock, C., Liu, X., Heneghan, R., Tittensor, D., Maury, O., Büchner, M., Vogt, T., Wang, T., Sun, F., Sauer, I. J., Koch, J., Vanderkelen, I., Jägermeyr, J., Müller, C., Rabin, S., Klar, J., Vega del Valle, I. D., Lasslop, G., Chadburn, S., Burke, E., Gallego-Sala, A., Smith, N., Chang, J., Hantson, S., Burton, C., Gädeke, A., Li, F., Gosling, S. N., Müller Schmied, H., ~~et al~~[Hattermann, F., Wang, J., Yao, F., Hickler, T., Marcé, R., Pierson, D., Thiery, W., Mercado-Bettín, D., Ladwig, R., Ayala-Zamora, A. I., Forrest, M., and Bechtold, M.](https://doi.org/10.5194/gmd-17-1-2024): Scenario setup and forcing data for impact model evaluation and impact attribution within the third round of the Inter-Sectoral Model Intercomparison Project (ISIMIP3a), *Geoscientific Model Development*, 17, 1–51, <https://doi.org/10.5194/gmd-17-1-2024>, 2024.
- 1040 Gilbert, M., Nicolas, G., Cinardi, G., Van Boeckel, T. P., Vanwambeke, S. O., Wint, G. R. W., and Robinson, T. P.: Global distribution data for cattle, buffaloes, horses, sheep, goats, pigs, chickens and ducks in 2010, *Sci Data*, 5, 180227, <https://doi.org/10.1038/sdata.2018.227>, 2018.
- 1050 Gupta, H. V., Kling, H., Yilmaz, K. K., and Martinez, G. F.: Decomposition of the mean squared error and NSE performance criteria: Implications for improving hydrological modelling, *Journal of Hydrology*, 377, 80–91, <https://doi.org/10.1016/j.jhydrol.2009.08.003>, 2009.
- [Hanasaki, N., Matsuda, H., Fujiwara, M., Hirabayashi, Y., Seto, S., Kanae, S., and Oki, T.: Toward hyper-resolution global hydrological models including human activities: application to Kyushu island, Japan, *Hydrology and Earth System Sciences*, 26, 1953–1975, <https://doi.org/10.5194/hess-26-1953-2022>, 2022.](https://doi.org/10.5194/hess-26-1953-2022)
- 1055 [Hannaford, J. and Marsh, T.: An assessment of trends in UK runoff and low flows using a network of undisturbed catchments, *International Journal of Climatology*, 26, 1237–1253, <https://doi.org/10.1002/joc.1303>, 2006.](https://doi.org/10.1002/joc.1303)
- 1060 Harrigan, S., Zsoter, E., Alfieri, L., Prudhomme, C., Salamon, P., Wetterhall, F., Barnard, C., Cloke, H., and Pappenberger, F.: GloFAS-ERA5 operational global river discharge reanalysis 1979–present, *Earth System Science Data*, 12, 2043–2060, <https://doi.org/10.5194/essd-12-2043-2020>, 2020.
- 1065 Hengl, T., Jesus, J. M. de, MacMillan, R. A., Batjes, N. H., Heuvelink, G. B. M., Ribeiro, E., Samuel-Rosa, A., Kempen, B., Leenaars, J. G. B., Walsh, M. G., and Gonzalez, M. R.: SoilGrids1km — Global Soil Information Based on Automated Mapping, *PLOS ONE*, 9, e105992, <https://doi.org/10.1371/journal.pone.0105992>, 2014.

Kohn, I., Stahl, K., and Stölzle, M.: Low Flow Events - a review in the context of climate change in Switzerland. Hydro-CH2018 Project, <https://doi.org/10.6094/UNIFR/150448>, 2019.

1115 Kreibich, H., Blauhut, V., Aerts, J. C. J. H., Bouwer, L. M., Van Lanen, H. A. J., Mejia, A., Mens, M., and Van Loon, A. F.: How to improve attribution of changes in drought and flood impacts, *Hydrological Sciences Journal*, 64, 1–18, <https://doi.org/10.1080/02626667.2018.1558367>, 2019.

Kumar, R., Samaniego, L., and Attinger, S.: Implications of distributed hydrologic model parameterization on water fluxes at multiple scales and locations, *Water Resources Research*, 49, 360–379, <https://doi.org/10.1029/2012WR012195>, 2013.

1120 Lange, S.: Trend-preserving bias adjustment and statistical downscaling with ISIMIP3BASD (v1.0). *Geoscientific Model Development Discussions*, 1–24, <https://doi.org/10.5194/gmd-2019-36>, 2019.

Lange, S., Quesada-Chacón, D., Büchner, M.: Secondary ISIMIP3b bias-adjusted atmospheric climate input data (v1.4). *ISIMIP Repository*. <https://doi.org/10.48364/ISIMIP.581124.4>, 2024.

1125 Lehner, B., Liermann, C. R., Revenga, C., Vörösmarty, C., Fekete, B., Crouzet, P., Döll, P., Endejan, M., Frenken, K., Magome, J., Nilsson, C., Robertson, J. C., Rödel, R., Sindorf, N., and Wisser, D.: High-resolution mapping of the world’s reservoirs and dams for sustainable river-flow management, *Frontiers in Ecology and the Environment*, 9, 494–502, <https://doi.org/10.1890/100125>, 2011.

Li, X., Zhou, Y., Hejazi, M., Wise, M., Vernon, C., Iyer, G., and Chen, W.: Global urban growth between 1870 and 2100 from integrated high resolution mapped data and urban dynamic modeling, *Communications Earth & Environment*, 2, 1–10, <https://doi.org/10.1038/s43247-021-00273-w>, 2021.

1130 Lin, P., Pan, M., Beck, H. E., Yang, Y., Yamazaki, D., Frasson, R., David, C. H., Durand, M., Pavelsky, T. M., Allen, G. H., Gleason, C. J., and Wood, E. F.: Global Reconstruction of Naturalized River Flows at 2.94 Million Reaches, *Water Resources Research*, 55, 6499–6516, <https://doi.org/10.1029/2019WR025287>, 2019.

1135 LISFLOOD static and parameter maps for Europe: <http://data.europa.eu/89h/f572c443-7466-4adf-87aa-c0847a169f23>, last access: 11 January 2024.

LISFLOOD OS online documentation: <https://ec-jrc.github.io/lisflood/>, last access: 15 December 2023.

LISVAP online documentation: <https://ec-jrc.github.io/lisflood-lisvap/>, last access: 15 December 2023.

1140 Mahto, S. S. and Mishra, V.: Does ERA-5 Outperform Other Reanalysis Products for Hydrologic Applications in India?, *Journal of Geophysical Research: Atmospheres*, 124, 9423–9441, <https://doi.org/10.1029/2019JD031155>, 2019.

McClean, F., Dawson, R., and Kilsby, C.: Intercomparison of global reanalysis precipitation for flood risk modelling, *Hydrology and Earth System Sciences*, 27, 331–347, <https://doi.org/10.5194/hess-27-331-2023>, 2023.

1145 Mentaschi, L., Alfieri, L., Dottori, F., Cammalleri, C., Bisselink, B., Roo, A. D., and Feyen, L.: Independence of future changes of river runoff in Europe from the pathway to global warming, *Climate*, 8, <https://doi.org/10.3390/cli8020022>, 2020.

1150 Merz, B., Blöschl, G., Vorogushyn, S., Dottori, F., Aerts, J. C. J. H., Bates, P., Bertola, M., Kemter, M., Kreibich, H., Lall, U., and Macdonald, E.: Causes, impacts and patterns of disastrous river floods, *Nat Rev Earth Environ*, 2, 592–609, <https://doi.org/10.1038/s43017-021-00195-3>, 2021.

- Muñoz-Sabater, J., Dutra, E., Agustí-Panareda, A., Albergel, C., Arduini, G., Balsamo, G., Boussetta, S., Choulga, M., Harrigan, S., Hersbach, H., Martens, B., Miralles, D. G., Piles, M., Rodríguez-Fernández, N. J., Zsoter, E., Buontempo, C., and Thépaut, J.-N.: ERA5-Land: a state-of-the-art global reanalysis dataset for land applications, *Earth Syst. Sci. Data*, 13, 4349–4383, <https://doi.org/10.5194/essd-13-4349-2021>, 2021.
- 1155 Nash, J. E. and Sutcliffe, J. V.: River flow forecasting through conceptual models part I — A discussion of principles, *Journal of Hydrology*, 10, 282–290, [https://doi.org/10.1016/0022-1694\(70\)90255-6](https://doi.org/10.1016/0022-1694(70)90255-6), 1970.
- 1160 Nilsson, C., Reidy, C. A., Dynesius, M., and Revenga, C.: Fragmentation and Flow Regulation of the World's Large River Systems, *Science*, 308, 405–408, <https://doi.org/10.1126/science.1107887>, 2005.
- [O'Neill, M. M. F., Tijerina, D. T., Condon, L. E., and Maxwell, R. M.: Assessment of the ParFlow-CLM CONUS 1.0 integrated hydrologic model: evaluation of hyper-resolution water balance components across the contiguous United States, *Geoscientific Model Development*, 14, 7223–7254, <https://doi.org/10.5194/gmd-14-7223-2021>, 2021.](https://doi.org/10.5194/gmd-14-7223-2021)
- 1165 Paprotny, D. and Mengel, M.: Population, land use and economic exposure estimates for Europe at 100 m resolution from 1870 to 2020, *Sci Data*, 10, 372, <https://doi.org/10.1038/s41597-023-02282-0>, 2023.
- Paprotny, D., Terefenko, P., and Śledziowski, J.: An improved database of flood impacts in Europe, 1870–2020: HANZE v2.1, *Earth System Science Data Discussions*, 1–37, <https://doi.org/10.5194/essd-2023-321>, 2023.
- 1170 Peña-Angulo, D., Vicente-Serrano, S. M., Domínguez-Castro, F., Lorenzo-Lacruz, J., Murphy, C., Hannaford, J., Allan, R. P., Tramblay, Y., Reig-Gracia, F., and El Kenawy, A.: The Complex and Spatially Diverse Patterns of Hydrological Droughts Across Europe, *Water Resources Research*, 58, e2022WR031976, <https://doi.org/10.1029/2022WR031976>, 2022.
- 1175 Pfahl, S. and Wernli, H.: Quantifying the relevance of ~~eyelonesatmospheric blocking~~ ~~precipitation~~ ~~co-located temperature~~ extremes, ~~*J. Climate*, 25, 6770–6780 in the Northern Hemisphere on (sub-)daily time scales, *Geophysical Research Letters*, 39, <https://doi.org/10.1029/2012GL052261>, 2012.~~
- 1180 Prudhomme, C., Parry, S., Hannaford, J., Clark, D. B., Hagemann, S., and Voss, F.: How Well Do Large-Scale Models Reproduce Regional Hydrological Extremes in Europe?, *Journal of Hydrometeorology*, 12, 1181–1204, <https://doi.org/10.1175/2011JHM1387.1>, 2011.
- Richards, N. and Gutierrez-Arellano, C.: Effects of community-based water management decisions at catchment scale, an interdisciplinary approach: the case of the Great Ruaha River Catchment, Tanzania, *Water Practice and Technology*, 17, 598–611, <https://doi.org/10.2166/wpt.2022.010>, 2022.
- 1185 [Samaniego, L., Kumar, R., and Attinger, S.: Multiscale parameter regionalization of a grid-based hydrologic model at the mesoscale, *Water Resources Research*, 46, <https://doi.org/10.1029/2008WR007327>, 2010.](https://doi.org/10.1029/2008WR007327)
- [Sajikumar, N. and Remya, R. S.: Impact of land cover and land use change on runoff characteristics, *Journal of Environmental Management*, 161, 460–468, <https://doi.org/10.1016/j.jenvman.2014.12.041>, 2015.](https://doi.org/10.1016/j.jenvman.2014.12.041)
- 1190 Sauer, I. J., Reese, R., Otto, C., Geiger, T., Willner, S. N., Guillod, B. P., Bresch, D. N., and Frieler, K.: Climate signals in river flood damages emerge under sound regional disaggregation, *Nat Commun*, 12, 2128, <https://doi.org/10.1038/s41467-021-22153-9>, 2021.

- 1195 Schellekens, J., Dutra, E., Weiland, F. S., Minvielle, M., Calvet, J.-C., Decharme, B., Eisner, S., Fink, G., Flörke, M., Peßenteiner, S., van Beek, R., Polcher, J., Beck, H., Orth, R., Calton, B., Burke, S., Dorigo, W., Weedon, G. P., and Delft, H.: A global water resources ensemble of hydrological models: the earth2Observe Tier-1 dataset, 2017.
- Schiavina, M., Freire, S., and MacManus, K.: GHS-POP R2019A - GHS population grid multitemporal (1975-1990-2000-2015) (R2019A), ~~[dataset]~~ https://ghsl.jrc.ec.europa.eu/ghs_pop2019.php, ~~[dataset]~~, 2019.
- 1200 Scussolini, P., Luu, L. N., Philip, S., Berghuijs, W. R., Eilander, D., Aerts, J. C. J. H., Kew, S. F., van Oldenborgh, G. J., Toonen, W. H. J., Volkholz, J., and Coumou, D.: Challenges in the attribution of river flood events, *WIREs Climate Change*, [n/a15](https://doi.org/10.1002/wcc.874), e874, <https://doi.org/10.1002/wcc.874>, [20232024](https://doi.org/10.1002/wcc.874).
- Sood, A. and Smakhtin, V.: Global hydrological models: a review, *Hydrological Sciences Journal*, 60, 549–565, <https://doi.org/10.1080/02626667.2014.950580>, 2015.
- 1205 Speckhann, G. A., Kreibich, H., and Merz, B.: Inventory of dams in Germany, *Earth System Science Data*, 13, 731–740, <https://doi.org/10.5194/essd-13-731-2021>, 2021.
- ~~Stahl, K., Tallaksen, L. M., Hannaford, J., and van Lanen, H. A. J.: Filling the white space on maps of European runoff trends: estimates from a multi-model ensemble, *Hydrol. Earth Syst. Sci.*, 16, 2035–2047, <https://doi.org/10.5194/hess-16-2035-2012>, 2012.~~
- 1210 Thiemig, V., Gomes, G. N., Skøien, J. O., Ziese, M., Rauthe-Schöch, A., Rustemeier, E., Rehfeldt, K., Walawender, J. P., Kolbe, C., Pichon, D., Schweim, C., and Salamon, P.: EMO-5: a high-resolution multi-variable gridded meteorological dataset for Europe, *Earth System Science Data*, 14, 3249–3272, <https://doi.org/10.5194/essd-14-3249-2022>, 2022.
- ~~Thober, S., Cuntz, M., Kelbling, M., Kumar, R., Mai, J., and Samaniego, L.: The multiscale routing model mRM v1.0: simple river routing at resolutions from 1 to 50 km, *Geoscientific Model Development*, 12, 2501–2521, <https://doi.org/10.5194/gmd-12-2501-2019>, 2019~~
- 1215 Tilloy, A., Malamud, B. D., and Joly-Laugel, A.: A methodology for the spatiotemporal identification of compound hazards: wind and precipitation extremes in Great Britain (1979–2019), *Earth System Dynamics*, 13, 993–1020, <https://doi.org/10.5194/esd-13-993-2022>, 2022.
- ~~1220 Tilloy, Alois; Paprotny, Dominik; Feyen, Luc; Grimaldi, Stefania; Gomes, Goncalo; Beck, Hylke; Lange, Stefan; Bianchi, Alessandra : HERA: a high resolution pan-European hydrological reanalysis (1950-2020). European Commission, Joint Research Centre (JRC) [dataset] PID: <http://data.europa.eu/89h/a605a675-9444-4017-8b34-d66be5b18e95>, 2024:~~
- 1225 Tomkins, K. M.: Uncertainty in streamflow rating curves: methods, controls and consequences, *Hydrological Processes*, 28, 464–481, <https://doi.org/10.1002/hyp.9567>, 2014.
- Tramblay, Y., Arnaud, P., Artigue, G., Lang, M., Paquet, E., Neppel, L., and Sauquet, E.: Changes in Mediterranean flood processes and seasonality, *Hydrology and Earth System Sciences*, 27, 2973–2987, <https://doi.org/10.5194/hess-27-2973-2023>, 2023.
- ~~1230 Van Lanen, H. a. J., Wanders, N., Tallaksen, L. M., and Van Loon, A. F.: Hydrological drought across the world: impact of climate and physical catchment structure, *Hydrology and Earth System Sciences*, 17, 1715–1732, <https://doi.org/10.5194/hess-17-1715-2013>, 2013.~~
- Van Loon, A.: Hydrological drought explained, *Wiley Interdisciplinary Reviews: Water*, 2, 359–392, <https://doi.org/10.1002/wat2.1085>, 2015.

- 1235 Vanham, D., Alfieri, L., Flörke, M., Grimaldi, S., Lorini, V., Roo, A. de, and Feyen, L.: The number of people exposed to water stress in relation to how much water is reserved for the environment: a global modelling study, *The Lancet Planetary Health*, 5, e766–e774, [https://doi.org/10.1016/S2542-5196\(21\)00234-5](https://doi.org/10.1016/S2542-5196(21)00234-5), 2021.
- Vanham, D., Alfieri, L., and Feyen, L.: National water shortage for low to high environmental flow protection, *Sci Rep*, 12, 3037, <https://doi.org/10.1038/s41598-022-06978-y>, 2022.
- 1240 Vassolo, S. and Döll, P.: Global-scale gridded estimates of thermoelectric power and manufacturing water use, *Water Resources Research*, 41, <https://doi.org/10.1029/2004WR003360>, 2005.
- Wada, Y., Flörke, M., Hanasaki, N., Eisner, S., Fischer, G., Tramberend, S., Satoh, Y., van Vliet, M. T. H., Yillia, P., Ringler, C., Burek, P., and Wiberg, D.: Modeling global water use for the 21st century: the Water Futures and Solutions (WFaS) initiative and its approaches, *Geoscientific Model Development*, 9, 175–222, <https://doi.org/10.5194/gmd-9-175-2016>, 2016.
- 1245 Wood, E. F., Roundy, J. K., Troy, T. J., van Beek, L. P. H., Bierkens, M. F. P., Blyth, E., de Roo, A., Döll, P., Ek, M., Famiglietti, J., Gochis, D., van de Giesen, N., Houser, P., Jaffé, P. R., Kollet, S., Lehner, B., Lettenmaier, D. P., Peters-Lidard, C., Sivapalan, M., Sheffield, J., Wade, A., and Whitehead, P.: Hyperresolution global land surface modeling: Meeting a grand challenge for monitoring Earth’s terrestrial water, *Water Resources Research*, 47, 2010WR010090, <https://doi.org/10.1029/2010WR010090>, 2011.
- Yamazaki, D.: CaMa-Flood, ~~[software] — <http://hydro.iis.u-tokyo.ac.jp/~yamada/cama-flood/index.html>, 2023-2023.~~
- 1255 Yamazaki, D., Ikeshima, D., Sosa, J., Bates, P. D., Allen, G. H., and Pavelsky, T. M.: MERIT Hydro: A High-Resolution Global Hydrography Map Based on Latest Topography Dataset, *Water Resources Research*, 55, 5053–5073, <https://doi.org/10.1029/2019WR024873>, 2019.
- 1260 Yang, Y., Pan, M., Lin, P., Beck, H. E., Zeng, Z., Yamazaki, D., David, C. H., Lu, H., Yang, K., Hong, Y., and Wood, E. F.: Global Reach-Level 3-Hourly River Flood Reanalysis (1980–2019), *Bulletin of the American Meteorological Society*, 102, E2086–E2105, <https://doi.org/10.1175/BAMS-D-20-0057.1>, 2021.
- Yu, Q., You, L., Wood-Sichra, U., Ru, Y., Joglekar, A. K. B., Fritz, S., Xiong, W., Lu, M., Wu, W., and Yang, P.: A cultivated planet in 2010 – Part 2: The global gridded agricultural-production maps, *Earth System Science Data*, 12, 3545–3572, <https://doi.org/10.5194/essd-12-3545-2020>, 2020.
- 1265 ~~Zajac, Z., Zambrano-Bigiarini, M., Salamon, P., Burek, P., Gentile, A., and Bianchi, A.: Calibration of the LISFLOOD hydrological model for Europe, https://www.efas.eu/sites/default/files/Manuals/JRC87717_efas_calibration_report%20final_9_jan_2014.pdf, last access: 15 January 2024, 2013.~~
- 1270 ~~Zajac, Z.,~~ Revilla-Romero, B., Salamon, P., Burek, P., Hirpa, F. A., and Beck, H.: The impact of lake and reservoir parameterization on global streamflow simulation, *Journal of Hydrology*, 548, 552–568, <https://doi.org/10.1016/j.jhydrol.2017.03.022>, 2017.